A major perturbation of the carbon cycle before the Ghaub glaciation (Neoproterozoic) in Namibia: Prelude to snowball Earth?

Galen P. Halverson, Paul F. Hoffman, and Daniel P. Schrag

Department of Earth and Planetary Sciences, Harvard University, Cambridge, Massachusetts 02138, USA
(halvers@eps.harvard.edu; hoffman@eps.harvard.edu; schrag@eps.harvard.edu)

Alan J. Kaufman

Department of Geology, University of Maryland, College Park, Maryland 20742, USA
(kaufman@geol.umd.edu)

[1] A large (11–15‰) negative shift in $\delta^{13}C$ is observed in shallow water carbonates directly beneath Neoproterozoic glacial deposits (or correlative disconformity) in northwest Namibia ascribed to a snowball Earth. Reproducibility and stratigraphic concordance of this anomaly in 16 sections across the ancient continental shelf support a primary origin, and field relations show it predates the fall in sea level associated with the Ghaub glaciation. We crudely estimate the duration of the isotopic shift as $\sim 0.6 \times 10^6$ years from a simple thermal subsidence model. Similar or larger $\delta^{13}C$ anomalies are found directly beneath Neoproterozoic glacial units in Australia, Canada, China, Scotland, and Svalbard. After considering conventional interpretations for negative $\delta^{13}C$ anomalies, we conclude that a prolonged methane release to the atmosphere is most consistent with the timescale, magnitude, and geological context of the anomaly in Namibia. Counterintuitively, an anomalous methane flux that is sustained for 100s kyr may be consistent with a snowball glaciation.

1. Introduction

[2] Late Neoproterozoic (roughly 600–700 Ma) glacial deposits are found worldwide [*Evans*, 2000], even on stable platforms composed of thick carbonate strata [*Hambrey and Harland*, 1981]. The association of negative $\delta^{13}C$ anomalies with carbonates that characteristically "cap" the glacial deposits is well established [*Kaufman et al.*, 1997]. These negative anomalies contrast sharply with the

highly ^{13}C-enriched composition of Neoproterozoic carbonates as a whole. The depletion in ^{13}C observed in cap carbonates is consistent with the snowball Earth hypothesis [*Kirschvink*, 1992a; *Hoffman et al.*, 1998a]. According to this hypothesis, major Neoproterozoic glaciations were global or near-global events, initiated by runaway ice-albedo feedback and terminated after prolonged buildup of atmospheric CO_2 due to normal volcanic outgassing but greatly reduced silicate weathering. *Hoffman et al.* [1998a] interpreted the isotopic signature of cap carbonates to be a consequence of prolonged low organic productivity during snowball events, high rates of carbonate sedimentation due to intense carbonate and silicate weathering in the ultragreenhouse aftermaths, and/or Rayleigh distillation of the atmospheric carbon source as the large CO_2 reservoir is transferred rapidly to the ocean.

[3] A large (11–15‰) negative $\delta^{13}C$ anomaly of regional extent found in carbonates directly beneath the Ghaub glacial deposits (or correlative disconformity) in Namibia [*Hoffman et al.*, 1998a] is more difficult to understand. Of the three causes of negative $\delta^{13}C$ anomalies in cap carbonates offered by *Hoffman et al.* [1998a], only the first (low productivity) could conceivably apply prior to runaway glaciation. This explanation is problematic, however, as primary productivity in the tropical ocean should have continued as long as it was ice-free, even if polar ice caps reached the midlatitudes. Runaway ice-albedo feedback would have finally closed the tropical ocean too rapidly [*Hyde et al.*, 2000] for $\delta^{13}C$ to change significantly. Moreover, a decline in productivity would reduce the uptake of CO_2, causing pCO_2 to rise, mitigating against an ice age. The subglacial isotopic shift in Namibia is not an isolated occurrence; $\delta^{13}C$ also drops beneath Neoproterozoic glacial deposits in South Australia [*McKirdy et al.*, 2001; *Walter et al.*, 2000], the northern Canadian Cordillera [*Narbonne et al.*, 1994; *Kaufman et al.*, 1997], northeastern Svalbard [*Fairchild and Spiro*, 1987; *Kaufman et al.*, 1997], Scotland [*Brasier and Shields*, 2000], and northwestern China [*Xiao et al.*, 2001]. These perturbations are tantalizing because they may shed light on conditions that set the stage for snowball glaciation.

[4] This paper is part of a larger study of the Otavi Group in Namibia, a well-exposed, carbonate-dominated succession of Neoproterozoic age (∼600–760 Ma) that hosts two discrete glacigenic intervals, the younger of which is the Ghaub Formation. Here we document the regional extent of the pre-Ghaub isotopic anomaly and its sequence-stratigraphic context across different paleobathymetric zones (inner shelf, outer shelf and upper slope). The isotopic shift occurs across a stratigraphic interval 20–50 m thick in pure carbonates of the upper Ombaatjie Formation. It is discordant with and older than the glacial erosion surface at the top of the formation. The timescale of the shift cannot be constrained radiometrically or magnetostratigraphically but only by assuming an average sediment accumulation rate. To this end, we argue that the rift-drift tectonic transition in the platformal succession is best placed at the base of the Ombaatjie Formation, meaning that the isotopic shift occurred early in the thermally driven subsidence stage. Using an estimated crustal stretching factor (β) of 1.2, we derive a thermal subsidence model, from which we infer that the duration of the isotopic shift was likely within a factor of two of $\sim 0.6 \times 10^6$ years. We then consider various explanations for the isotopic shift, bearing in mind its estimated duration and the ensuing catastrophic glaciation. We conclude that the data best support a new, counterintuitive hypothesis [*Schrag et al.*, 2002] involving methane as a climatic destabilizing agent, and a harbinger of the snowball Earth.

2. Regional Setting

[5] The Otavi Group drapes the southern promontory of the Congo Craton (Figure 1) in northwest Namibia [*Miller*, 1997] and is exposed for 800 km in a Pan-African fold belt that rims the craton [*Hedberg*, 1979]. The fold belt is defined by a tripartite Neoproterozoic succession (Figure 1d). At the base is the rift-clastic Nosib Group, known to be older than 756 ± 2 Ma [*Hoffman et al.*, 1996]. In the middle is the carbonate-dominated Otavi Group, which spans the rift-drift transition and
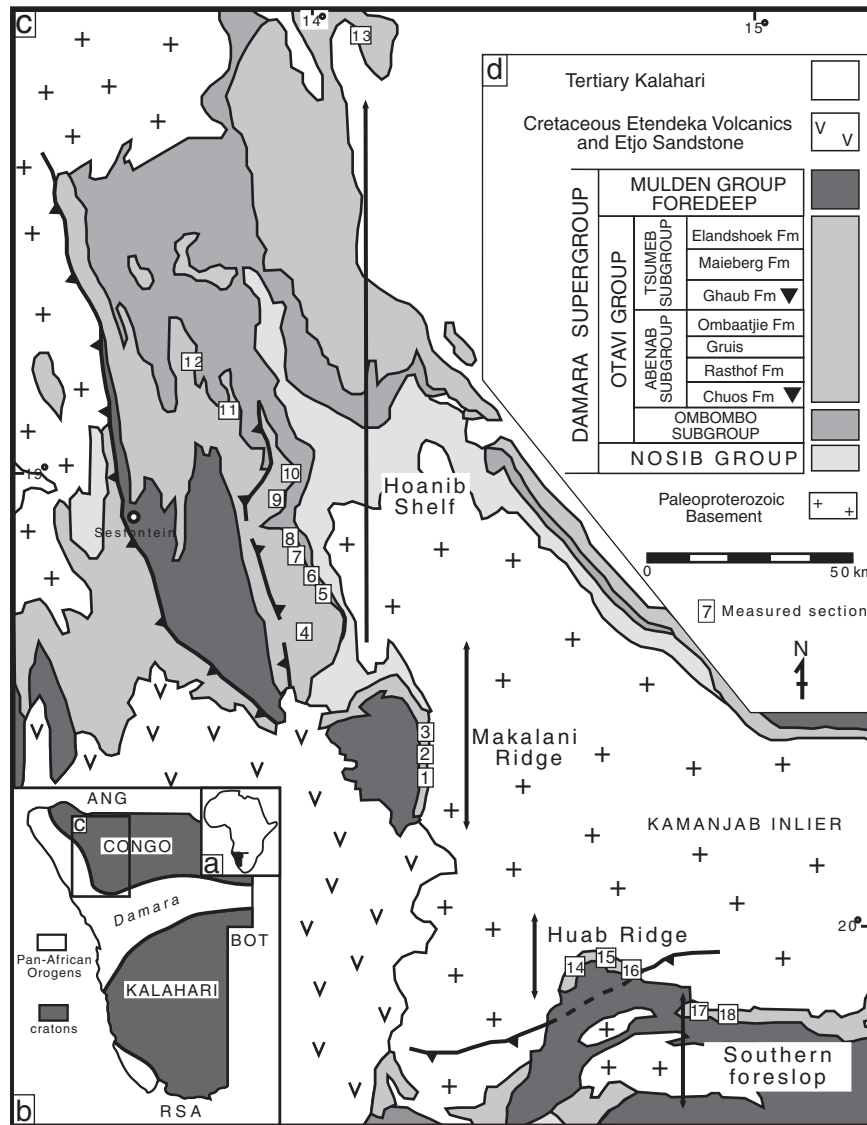
Figure 1. (a) Map of Africa showing location of Namibia. (b) Map of Namibia showing distribution of Neoproterozoic orogenic belts. Inset box shows location of map in Figure 1c. (c) Geological sketch map of northwest Namibia showing locations of measured sections (Figures 6–8). Arrows indicate paleogeographic divisions of the Otavi basin during deposition of the Ombaatjie Formation (see also Figure 2). (d) Legend for geological map, including a general stratigraphic column of the Otavi Group (see also Figure 2).

succeeding thermal-subsidence stage of a south-facing (in present coordinates) passive margin (Figure 2). The lower Otavi Group (Ombombo subgroup) contains volcanics in the south dated at 758 ± 4 and 746 ± 2 Ma [*Hoffman et al.*, 1996]. The Otavi Group is well exposed on the western and southern flanks of the Kamanjab basement (Paleoproterozoic) inlier, situated at the southwestern syntaxis of the fold belt (Figure 1). Its continuity is broken, however, by areas of erosional

truncation beneath the disconformably overlying Mulden Group and the flat-lying Cretaceous [*Frets*, 1969]. The Mulden Group is a siliciclastic foredeep sequence related to collision ~630–550 Ma with the active margin of the Rio Plata craton [*Stanistreet et al.*, 1991; *Alkmim et al.*, 2001]. Low-grade (anchizonal) metamorphism of the Mulden Group occurred ~535 Ma [*Clauer and Kröner*, 1979]. The fold belt has been pervasively remagnetized [*Evans*, 2000], but paleopoles obtained elsewhere
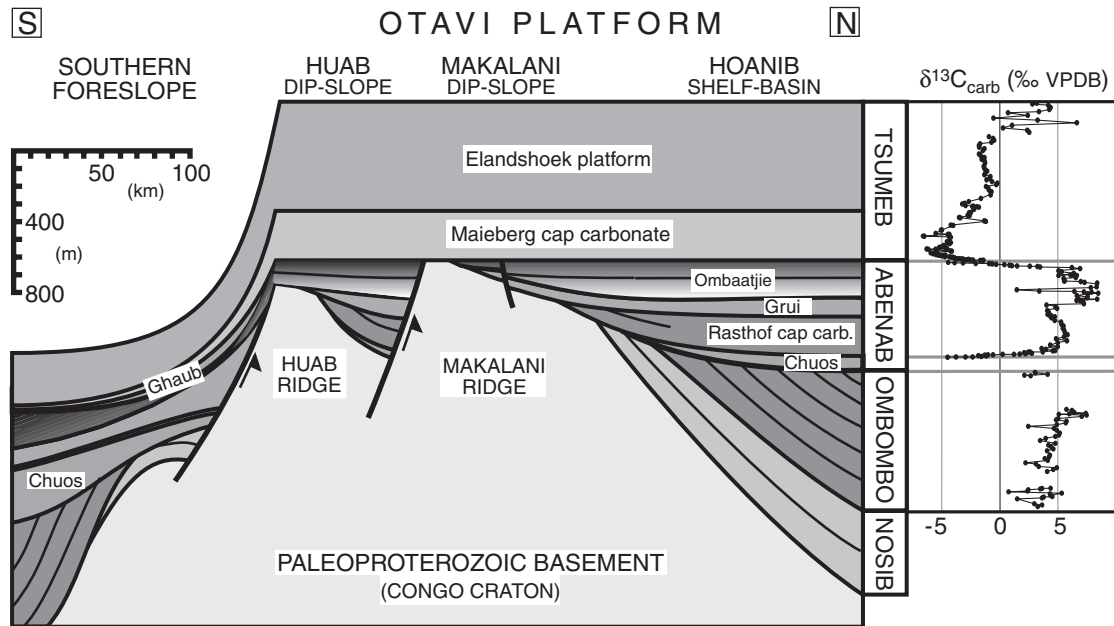
Figure 2. Schematic north-south cross section showing paleogeographic divisions of the Otavi basin and stratigraphic relationships across the rift-drift transition, as controlled by east-west trending basement uplifts (Huab and Makalani ridges). The Otavi basin is separated into the deepwater foreslope in the south and the Otavi platform to the north. The latter is further subdivided into the Huab dip slope (outer shelf) and Makalani dip slope and Hoanib shelf (inner shelf). The $\delta^{13}C$ profile is a composite of our own data from multiple sections on the Hoanib shelf. Gaps in the record represent siliciclastic and/or glacigenic sediments.

on the Congo craton [*Meert et al.*, 1995, 1996] provide paleolatitude estimates for our study area of ~10° at 743 ± 30 Ma and ~39°S at 547 ± 4 Ma [*Evans*, 2000] that loosely bracket the Neoproterozoic succession.

2.1. Otavi Group

[6] Early studies of the Otavi Group focused on the Otavi Mountains [*South African Committee for Stratigraphy (SACS)*, 1980], a famous mining district near the eastern end of the fold belt. To the west, the outer flanks of the Kamanjab inlier (Figure 1) were originally mapped by *Frets* [1969], *Guj* [1970], *Porada* [1974] and industry geologists. *Hedberg* [1979] used all these sources and original observations in his systematic overview of the entire fold belt. The first $\delta^{13}C$ data for the Otavi Group was obtained from drill cores in the Otavi Mountains [*Kaufman et al.*, 1991] and the preglacial negative shift was encountered, in one sample. To this point, all workers had assumed there was but one glacial formation of regional extent in the fold belt. They assigned it to the

Chuos Formation [*SACS*, 1980] and used it as the datum for regional correlations. Later, *Hoffmann and Prave* [1996], independently confirmed by us (P.F.H. and A.J.K.), showed that two discrete glacial formations exist. The major glacial deposits in the Otavi Mountains were reassigned to the younger, Ghaub Formation [*Hoffmann and Prave*, 1996]. This led to wholesale revision of regional correlations and to a broadly recognized sequence of formations (Figure 1; *Hoffmann and Prave* [1996], *Hoffman et al.* [1998b]). *Prave* [1996] proposed that foredeep subsidence began with the Ombaatjie Formation, which would invalidate our thermal subsidence model, but we find little support for this idea [see, also, *Dürr and Dingeldey*, 1997]. *Kennedy et al.* [1998, 2001a, 2001b] report data from the Otavi Group in two areas, one on the platform close to our measured section 8 and the other on the southern foreslope east of our measured section 18 (Figure 1).

[7] We use the threefold division of the Otavi Group into the Ombombo, Abenab and Tsumeb subgroups (Figure 1) proposed by *Hoffmann and*

Prave [1996]. The Abenab and Tsumeb subgroups are each floored by glacial deposits, the Chuos and Ghaub formations, respectively, or correlative disconformities (Figure 2). Both glacigenic intervals are sharply bounded and are overlain by lithologically and isotopically distinctive cap-carbonate sequences: the Rasthof and Maieberg formations, respectively [*Hoffman et al.*, 1998b]. Carbonates in the upper Ombombo and upper Abenab subgroups, preceding the glacial events, are strongly enriched in ^{13}C (Figure 2) as is the upper Tsumeb subgroup in the Otavi Mountains [*Kaufman et al.*, 1991], where it extends stratigraphically higher than in the west. The contrasting negative δ^{13}C anomaly upon which this paper is focused occurs at the top of the Abenab subgroup, in the upper Ombaatjie Formation.

[8] Our schematic cross section of the Otavi Group (Figure 2) incorporates the 18 measured sections (MS) used in this study (Figure 1), many supplementary sections, and stratigraphic cutoffs (onlaps and toplaps) documented by systematic mapping between all our sections. The cross section encapsulates the progressive differentiation of a shallow-water platform to the north and a contemporaneous deepwater slope and basin to the south. This zonation resulted from north-south crustal stretching of greater intensity and duration in the south [*Henry et al.*, 1990]. On the platform, stretching is manifested by syn-sedimentary uplift, back-rotation and erosion of two paleotopographic highs; the Huab and Makalani ridges [*Soffer*, 1998; *Hoffman and Hartz*, 1999]. We infer that the ridges originated by footwall uplift on south-dipping normal faults (Figure 2), although the faults cannot be directly observed because of stratigraphic overlap by the Mulden Group on the Huab ridge and by Cretaceous strata on the Makalani ridge (Figure 1). Block uplift and back rotation is indicated by erosional truncation on the upper dip slopes and concomitant shedding of basement- and cover-derived detritus onto the lower dip slopes. Projection of subgroup-boundary cutoffs across the Kamanjab inlier (Figure 1) suggests that the uplifts trend approximately east-west and parallel the southern margin of the Otavi platform and the Congo craton.

[9] Uplift first occurred during middle and upper Ombombo deposition and continued during the Chuos glaciation. The uplift is masked by the high sedimentation rate of the succeeding Rasthof cap-carbonate sequence [*Hoffman*, 2000]. Stretching culminated in middle Abenab time (Gruis Formation), when both ridges were strongly uplifted. The southern margin of the platform (Huab ridge) was permanently established at that time. The "rift-drift" transition on the platform corresponds essentially to the base of the Ombaatjie Formation, which has an apparent onlap relationship with respect to the inherited topography (Figure 2). This topography was buried by the middle Ombaatjie, although the Makalani ridge was reactivated one last time during the Ghaub glaciation when stronger crustal stretching and block rotation occurred in the Outjo basin south of the cross section.

[10] For paleogeographic simplicity, "inner shelf" refers to the area north of the Makalani ridge (MS 1–13), "outer shelf" corresponds to the Huab ridge (MS 14–16), and "southern foreslope" is the incline to the Outjo deepwater basin (MS 17–18).

2.2. Ombaatjie Formation

[11] The Ombaatjie (om-BUY-gee) Formation is the youngest unit in the Abenab subgroup and the substrate for the Ghaub glaciation (Figure 2). Our type section (MS 7) is on the inner shelf, near the village of Ombaatjie (19.3°S, 14.02°E) at the head of the Hoanib River. It is a typical shelf section, nearly 200 m thick, in which the lower half presents cliff-forming, dark grey limestone, and the upper half is less resistant, tan to medium grey dolomite. Shelf sections expose an aggradational stack of 6–8 depositional cycles (parasequences) with a mean thickness of ~25–30 m. The cycles are bounded by semi-continuous exposure surfaces and display condensed transgressive but complete regressive sets of lithofacies. There is considerable lateral variability within cycles, little of which appears systematic in the north-south section. On the Huab and Makalani dip slopes, the lower cycles disappear due to onlap, and the formation thins by up to half its normal thickness (~100 m).

[12] The Ombaatjie is easily distinguished from the underlying Gruis (KHRICE) Formation. On the Hoanib shelf (Figure 2), the Gruis is recessive and consists of multitudinous, sub-meter-scale cycles of tan to pinkish, marly dolomite. The cycles are characteristically topped by microbialaminite with well-developed, supratidal tepee structures [*Kendall and Warren*, 1987]. On the Huab and Makalani dip slopes, the same tepee dolomite facies caps tongues of basement-derived conglomerate and sandstone shed northward down slope (Figure 3a). The top of the Gruis is a mappable exposure surface that is abruptly transgressed by dark grey Ombaatjie limestone. This transition marks a shift to more prevalent, deeper water shelf facies and a sharp increase in mean cycle thickness. We interpret this change as indicating the onset of thermal subsidence on the platform.

[13] The top of the Ombaatjie Formation is also well defined. On the shelf, this surface is an erosional disconformity with up to ~70 m of relief regionally (Figures 6–8). The medium grey Ombaatjie dolomite is weakly brecciated and silicified at the erosion surface, which in most places is directly overlain by a contrasting, very pale cream-colored, cliff-forming dolomite. This is the transgressive Keilberg member of the Maieberg cap-carbonate sequence. The Keilberg dolomite is characteristically well-laminated, hummocky cross-stratified, and hosts a peculiar form of stromatolite [*Hoffman et al.*, 2002]. Although the glacigenic Ghaub Formation is commonly absent on the platform, <1.5 m of multicolored diamictite is sporadically preserved (Figure 3b) at or near MS 2, 4, 6, and 8 (Figure 1), which confirms unambiguously the separation of preglacial and postglacial strata in all sections.

[14] The Ombaatjie Formation is quite different on the southern foreslope (MS 17–18). The foreslope deposits lack exposure surfaces of any kind and consist exclusively of allodapic carbonate grain flows and fine debris flows. The base is placed arbitrarily at the top of the last significant siliciclastic turbidite interval, which we correlate with the upper Gruis Formation. The Abenab subgroup overall exhibits a high degree of stratigraphic variability along strike on the southern foreslope, which may

partly be due to large-scale submarine landsliding. The negative $\delta^{13}C$ composition (section 3.6) of the allodapic (redeposited) dolomite suggests that much of it is derived from the uppermost Ombaatjie Formation on the shelf, possibly due to sea level lowering at the onset of glaciation. The Ombaatjie slope deposits are overlain sharply by the Ghaub Formation (<140 m), consisting of glacigenic diamictites, coarse debris flows, and graded allodapic carbonates with numerous dropstones. Debris flows in the Ghaub are distinguished from those in the Ombaatjie by their heterolithic clast composition, abundant outsize clasts, and orange-weathering ferruginous dolomite matrix (Figure 3c).

3. Carbon Isotopes

[15] The summary $\delta^{13}C$ profile through the Otavi Group in Figure 2 is a composite section representing the Hoanib shelf [*Hoffman et al.*, 1998a; unpublished data, 2001]. The profile is in general agreement with that published by *Kennedy et al.* [1998] for the same area (their West Congo Craton, Entrance section). Most of the data presented here are new, but we do include previously published data [*Hoffman et al.*, 1998a] from MS 5–7, 11, 15, 17 and 18 (Figures 6–8). All $\delta^{13}C$ (and accompanying $\delta^{18}O$) data presented in this paper are available as auxillary material (available in the HTML version of the article at http://www.g-cubed.org).

3.1. Methods

[16] We collected fresh, clean samples from all the measured sections used in this study. The $\delta^{13}C$ and $\delta^{18}O$ were measured on powders microdrilled from slabbed and polished samples; Mn/Sr data presented in Figure 4 were measured using the same powders. Most isotope data were acquired simultaneously on a Micromass Optima dual inlet mass spectrometer attached to a modified Isocarb preparation device in the Harvard University Laboratory for Geochemical Oceanography (other new and previously published data were generated by a similar technique at Rocky Mountain Mass Spectrometry). Approximately 1 mg microdrilled samples were reacted in a common, purified H_3PO_4 bath at 90°C. Evolved CO_2 was collected cryogeni-

Figure 3. (a) East facing view of Otavi exposure on the Huab Ridge, at Tweelingskop (MS 14). Photo shows stratigraphic relationships [*Soffer*, 1998], including conglomerate wedges in the Gruis onlapping a rotated basement block and Rasthof Formation carbonate in the foreground (lower right) that is truncated beneath the Gruis conglomerate on the far wall. We interpret this region to represent the outer shelf rim, which explains the unique occurrence of the aeolianite in the upper Ombaatjie and reef buildups in the overlying Maieberg Fm. (cap carbonate). Owing to onlap, the Ombaatjie Formation comprises cycles 3–8 only. (b) Field photograph at Entrance (MS8) shows ~1 m of Ghaub diamicite separating the upper Ombaatjie Formation and the Keilberg Member of the Maieberg Formation ("cap" carbonate) on the Hoanib shelf. Geologist Marek Wendorf for scale. (c) Exposure of contact between Ombaatjie foreslope deposits and the Ghaub diamictite near Fransfontein (20°11.9'S, 15°02.0'E). Divisions on staff are 0.1 m, for scale.

cally and analyzed using a reference gas. External error (1σ) from standards was better than ±0.1‰ for both $\delta^{13}C$ and $\delta^{18}O$. Samples were calibrated to Vienna Peedee belemnite (VPDB) using an in-house Cararra Marble standard. The $\delta^{18}O$ was corrected for equilibrium with H_3PO_4 using the *Craig* [1957] equation. Potential memory effect resulting from the common acid-bath system was
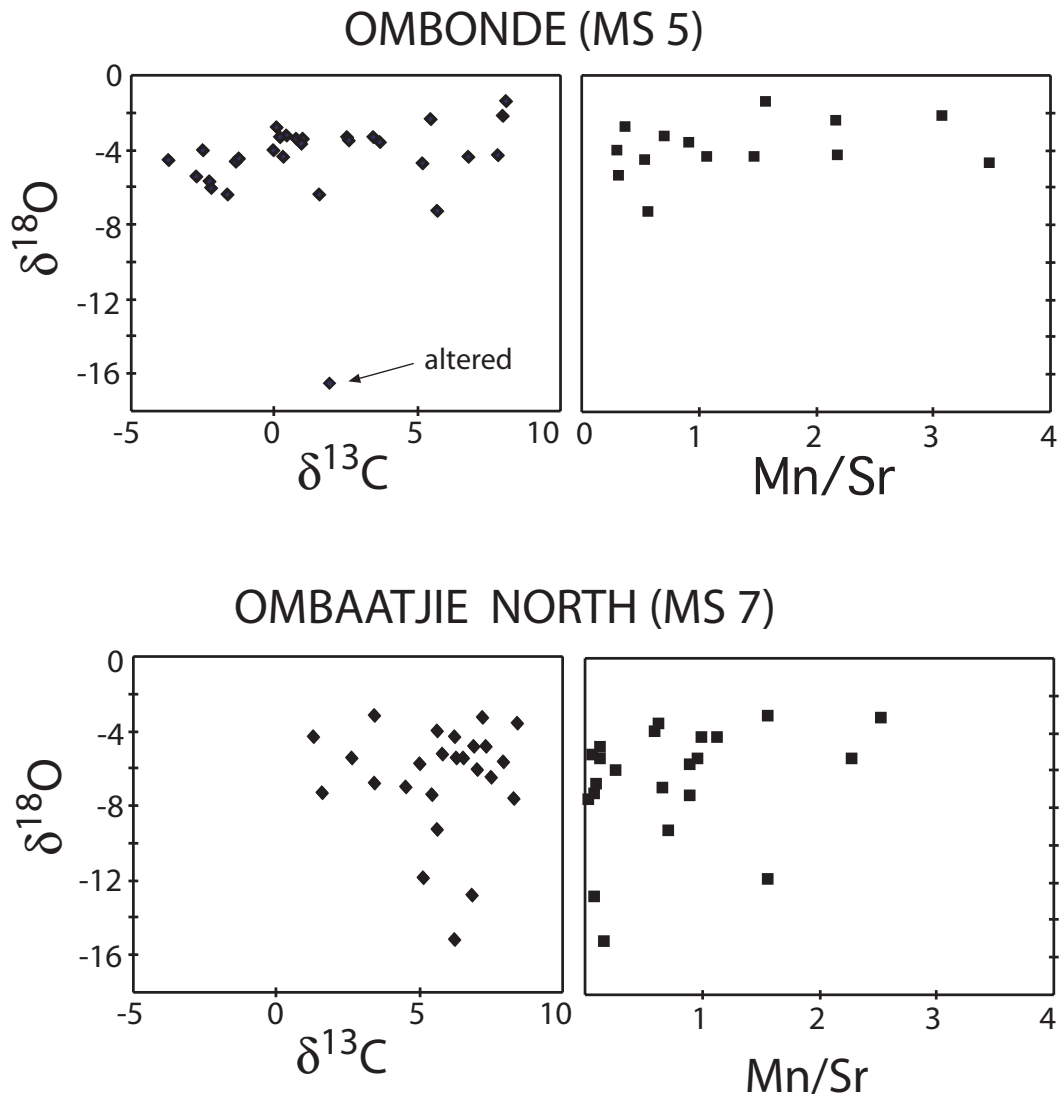
Figure 4. Crossplots of δ^{18} versus δ^{13}C (VPDB) and Mn/Sr for MS5 and MS7. Note the lack in correlation between δ^{18} and either δ^{13}C or Mn/Sr.

minimized by tripling the reaction time for dolomite samples and monitoring standards. Memory effect is estimated at <0.1‰ and <0.2‰ for δ^{13}C and δ^{18}O, respectively, based on variability of standards run after samples. Elemental analyses (Mn/Sr ratios) were performed on a PG PQ2+ plasma source quadrupole mass spectrometer at Harvard University. See *Kaufman et al.* [1993] for a detailed explanation of elemental analytical techniques.

3.2. Diagenetic Considerations

[17] Diagenesis is a concern in carbonate rocks that have undergone total recrystallization (to dolomite

or low-Mg calcite). The δ^{13}C is much less susceptible to alteration than δ^{18}O because the rock/water ratio with respect to carbon is much higher than for oxygen [*Banner and Hanson*, 1990]. Meteoric waters are depleted in ^{18}O compared with seawater, and δ^{18}O can therefore be used to screen for meteoric diagenesis. Mn/Sr is generally higher in meteoric waters than in seawater, so an inverse correlation between δ^{18}O and Mn/Sr is a strong indicator of meteoric diagenesis [*Brand and Veizer*, 1981; *Derry et al.*, 1992].

[18] Figure 4 shows cross-plots of δ^{18}O$-\delta^{13}$C and δ^{13}C-Mn/Sr for two measured sections. The lack of

	Facies	Lithology/ sedimentary features	Association/ environment
carbonate	Microbialamite	Microbially laminated, thin (<1 cm) and laterally discontinuous beds. Often contain teepee structures/breccias and intraclasts.	Supra- to intertidal flats, subject to frequent exposure and evaporitic conditions. Commonly cap shoaling-upward parasequences.
	Grainstone	Arenites, packstones, conglomerates. Clasts include ooids, reworked intraclasts, granules, and rounded mud pellets. Trough crossbeds are common. Sharp and scoured bases.	Shoals and shallow shelf, low- to high energy, current influenced, often gradtional laterally and vertically with stromatolites and ribbon rocks.
	Stromatolite	Branching, columnar, and conical stromatolites.	Mid- to outer-ramp and slope break, often laterally and vertically continuous with grainstones.
	Ribbonite	Mechanically deposited fine sands and silts in alternating mm to cm scale beds. Hummocky cross-stratification and "pinch and swell" structures common.	Subtidal, low energy, but storm influenced. Often gradational downward with rhythmites and upward and laterally with grainstones or stromatolites.
	Rhythmite	Fine grained, "rhythmic" laminae, fine upward and are typically continuous on the outcrop scale. Interbedded mm to cm scale allodaptic beds are the only indication of traction currents.	Offshore (outer ramp or slope), deep, quiet environments.
	Debris flow breccia	Variable sized tabular, rounded, or angular clasts in a fine-grained matrix.	Slope environment, interbedded with rhythmites
	Sandstone	Medium- to coarse-grained, poorly- to well-sorted; trough cross beds and scour surfaces common.	Marginal-marine, interbedded wtih argillite and siltstone.
	Shale and siltstone	Green, gray, and red, finely laminated silts, equivalent to the rhythmite facies.	Offshore (outer ramp or slope), deep, quiet environments.

Figure 5. Description of lithofacies used in stratigraphic sections (and legend to Figures 6–8).

any correlation between $\delta^{18}O$ and either $\delta^{13}C$ or Mn/Sr suggests that diagenesis was not dominantly meteoric. As an additional check, we measured $\delta^{13}C$ and $\delta^{18}O$ in brecciated and visibly altered samples related to paleo-exposure surfaces but found little significant difference (<1‰) in $\delta^{13}C$ compared with unaltered samples of the adjacent strata. We also avoided, where possible, sampling impure carbonates and carbonates that are interbedded with shale, in which $\delta^{13}C$ may be altered by metamorphic decarbonation reactions [*Wickham and Peters*, 1992] or reoxidation of organic matter [*Irwin et al.*, 1977]. Nevertheless, burial diagenesis and greenschist metamorphism likely had some effect on $\delta^{13}C$, and for this reason we only attach significance to shifts in $\delta^{13}C$ of more than 2‰ that are regionally reproduced.

3.3. Hoanib Shelf

[19] Figure 6 shows stratigraphic columns (see Figure 5 for legend) with $\delta^{13}C$ profiles of the Ombaatjie Formation on the Hoanib shelf (measured sections MS 4–13). The mean thickness of the Ombaatjie Formation on the shelf is ~200 m. Anomalous thin (MS 10) and thick (MS 12) sections lie east and west, respectively, of the general line of sections, which suggests that subsidence rates on the Hoanib shelf increased toward the presumed western margin of the craton. Reference section MS 7 is the most thoroughly sampled. Here the Ombaatjie Formation consists of seven cycles (parasequences), of which the first six have consistently heavy $\delta^{13}C$ values of +5 to +9‰. A minor drop to +2‰ occurs near the bottom of cycle 2 but does not appear in any other section. In cycle 7, $\delta^{13}C$ values decline regularly to almost 0‰ at the top of the section. The isotopic shift in cycle 7 is easily correlated with adjacent sections (Figures 6). In fact, the shift is more complete in other sections, where the full decline in $\delta^{13}C$ values approaches −4‰. The datum for Figure 6 is chosen arbitrarily at 0‰ on the $\delta^{13}C$ curve, which we infer to be isochronous. Correlation of cycle 7 across the shelf based upon the isotope curve illuminates, on the one hand, the aggradational character of the Ombaatjie cycles, and on the other hand, the lateral variability of lithofacies within cycles. There is no dependence of isotopic compositions on lithofacies.

[20] The correlation of cycle 7 also highlights the fact that the top of the Ombaatjie Formation, including the isotopic shift, is variably truncated (Figure 6). Clearly, the isotope shift predates the erosional disconformity. Interestingly, the inner shelf is more deeply eroded than the outer shelf (compare Figures 6, and 8). This erosion most
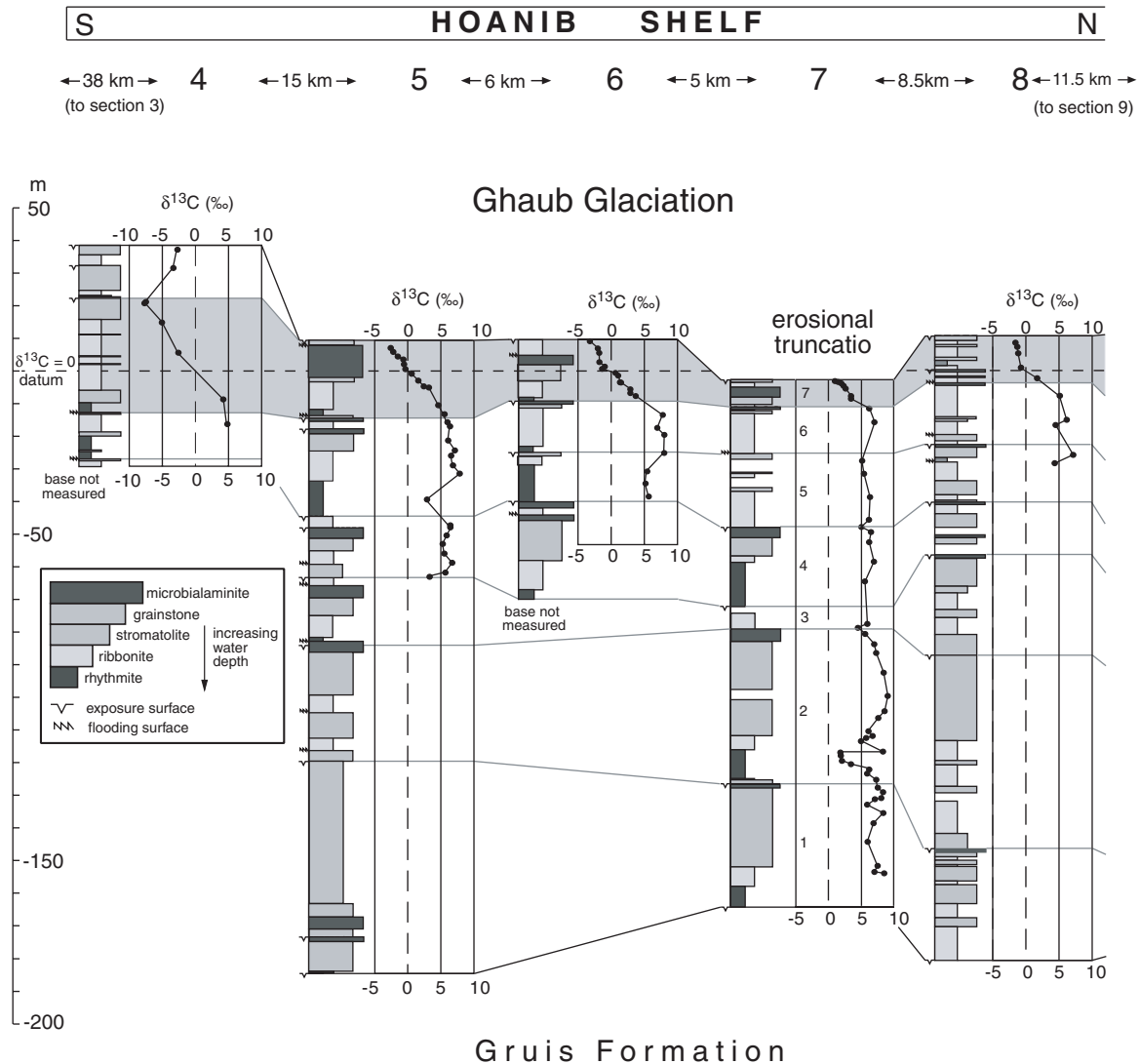
Figure 6. (a, b) Stratigraphic columns and $\delta^{13}C$ data (per mil VPDB) of the Ombaatjie Formation in Hoanib shelf-basin sections. Sections are numbered at the top of Figure 6, and locations are given in Figure 1. Cycles are defined based on reference section 7 (though note cycle 8 is missing here). All sections are hung on an arbitrarily chosen but presumably isochronous, "$\delta^{13}C = 0$" datum (projected in sections with sparse data) in order to illustrate the variable truncation/ preservation of cycles 7 and 8. Shaded boxes shows the correlation of cycle 7, which preserves the main part of the negative δ^{13} shift. Lower, thick black line represents the contact with underlying Gruis Formation, while the upper, thick, black line is the sub-Ghaub disconformity (glacial surface). Light gray correlation lines are discontinuous where correlation is uncertain. See Table 1 for description of facies. All $\delta^{13}C$ data and coordinates of measured sections are available as auxiliary material in the HTML version of the article (available at http://www.g-cubed.org).

likely occurred before the shelf was glaciated but after ice buildup elsewhere lowered sea level. In this event, the Ombaatjie inner shelf could be analogous to the present Belize carbonate shelf where "reversed" morphology is attributed to karstic erosion during Quaternary lowstands [*Purdy*, 1974]. The Ombaatjie foreslope grain and

debris flows (Figure 8) could represent the mechanical products of that erosion (section 3.6).

3.4. Makalani Dip Slope

[21] Above the Makalani dip slope, the Ombaatjie Formation thins and eventually disappears beneath
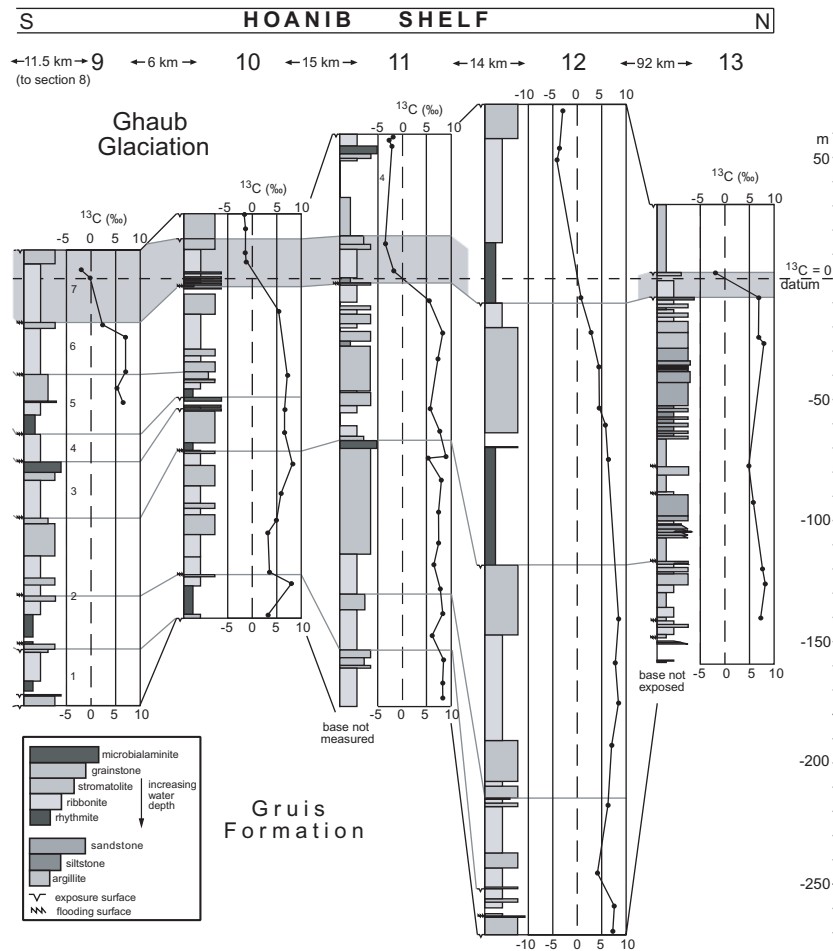
Figure 6. (continued)

the Maieberg cap-carbonate sequence (Figure 2). Two observations suggest that this is a result of depositional onlap, rather than erosional truncation as in the underlying syn-rift strata (Figure 2). The first observation is that, where the Ombaatjie Formation is <100 m thick (MS 1), the grainstone-dominated cycles 1 and 2 are missing (Figure 7). The second observation is that cycles 7, containing the negative $\delta^{13}C$ shift, and 8 persist. These observations show that the Ombaatjie Formation thins from the bottom up and not from the top down. In detail, the onlap is localized at a west-northwest-dipping normal fault that obliquely intersects the line of sections between MS 1 and 2 (Figure 7). This fault was active during Ombaatjie cycles 1−3 and again during the Ghaub glaciation.

[22] The upper Ombaatjie $\delta^{13}C$ shift is well documented in MS 2 (Figure 7). As on the Hoanib shelf, $\delta^{13}C$ declines smoothly upsection from greater than +5 to less than −3‰ in cycle 7 over an ∼20 m interval. The lower half of cycle 8 is argillaceous and was not sampled, but the upper half consists of limestone rhythmites and ribbonites in which $\delta^{13}C$ increases erratically from −7 to −3‰.

3.5. Huab Dip Slope

[23] Depositional onlap above the Huab dip slope also is indicated by truncation of the lower grainstone-dominated cycles and preservation of the upper Ombaatjie $\delta^{13}C$ deviation (Figure 8). The $\delta^{13}C$ values in cycles 3−6 hover near +5 to 6‰,
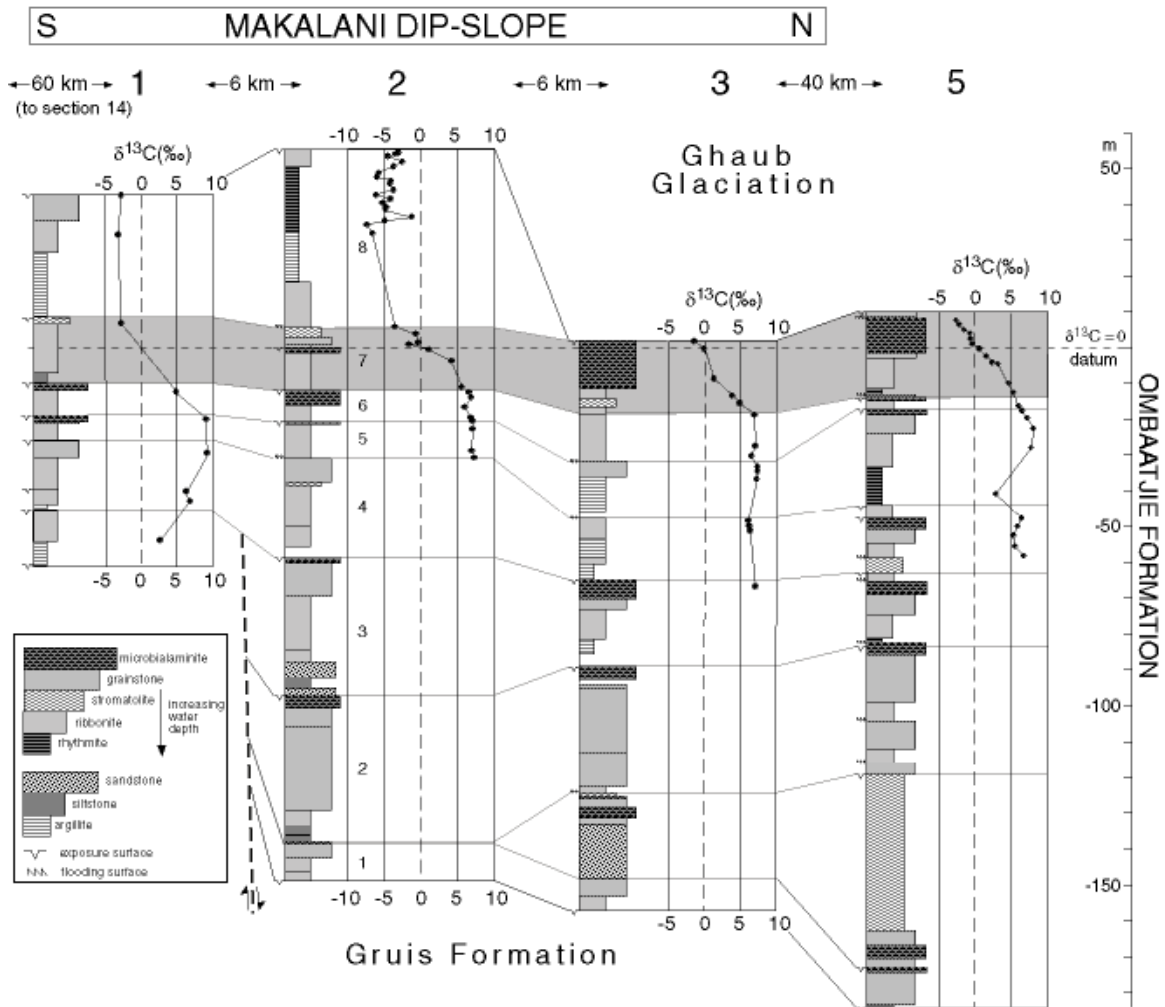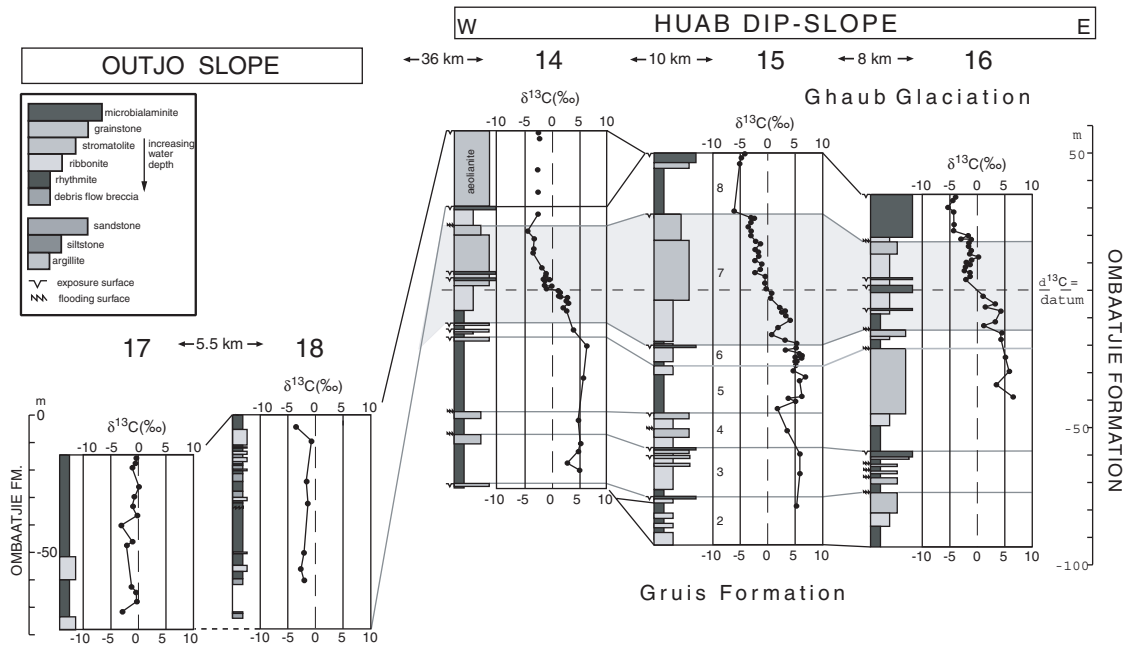
Figure 7. Stratigraphic columns and $\delta^{13}C$ from the Makalani dip slope. Like Figure 6, sections are hung from a "$\delta^{13}C = 0$" datum, the shaded box is cycle 7, and the lower and upper, thick black lines represent the Gruis contact and sub-Ghaub disconformity, respectively. Normal fault between sections 1 and 2 was active during deposition of cycles 1–3 and probably accounts for presence of sand tongues in the lower part of MS2-3. Absence of cycles 1–2 in MS1 shows southward onlap relationship onto the Makalani Ridge (see Figure 2). MS5 is from the Hoanib shelf (Figure 6a) and is duplicated here to show correlations between the Makalani dip slope and Hoanib shelf. All $\delta^{13}C$ data and coordinates of measured sections are available as auxillary material in the HTML version of the article (available at http://www.g-cubed.org).

which is ~2‰ lower than the equivalent interval on the inner shelf (see also Figure 10). The scatter in $\delta^{13}C$ values in the basal ~10 m of cycle 7 is probably diagenetic, related to a marly component. Thereafter, $\delta^{13}C$ values decline smoothly in pure carbonate to the top of cycle 7, which is marked by a prominent stromatolite biostrome also present on the Makalani dip slope (Figure 7). Cycle 7 is a composite parasequence in MS 14 and 16, but its thickness on the Huab dip slope (30–50 m) is similar to that on the

Hoanib shelf (20–40 m). The change in $\delta^{13}C$ in cycle 7 on the Huab dip slope is clearly independent of lithofacies.

[24] In cycle 8, negative $\delta^{13}C$ values stabilize near −4‰, similar to sections on the Makalani dip slope (MS 1, 2) and Hoanib shelf (MS 4, 10, 11). In MS 14 (Figure 3a and 8), the top 28 m of the Ombaatjie Formation consists of very homogeneous dolomite grainstone. Although strongly recrystallized, relic large-scale cross-bedding and centimeter-scale,

Figure 8. Stratigraphic columns and $\delta^{13}C$ data from Huab dip slope and foreslope (Outjo basin) sections. Like Figures 6 and 7, Huab dip slope sections are hung from a "$\delta^{13}C = 0$" datum, the shaded box is the correlation of cycle 7, and the lower and upper, thick black lines represent the Gruis contact and sub-Ghaub disconformity, respectively. Note that cycle 1 is everywhere absent here and that cycle 2 thins dramatically from MS15 to MS14. Correlation with the Outjo slope (MS17–18) is ambiguous, these sections only constrained (based on $\delta^{13}C$) to postdate deposition of the lower part of cycle 7 (i.e., after $\delta^{13}C$ drops below 0‰). Dashed line in MS18 represents the approximate contact with the underlying Gruis Fm. All $\delta^{13}C$ data and coordinates of measured sections are available as auxillary material in the HTML version of the article (available at http://www.g-cubed.org).

"pin-stripe" laminae defined by oscillatory grain-size gradations (normal and inverse graded) suggest an aeolian deposit. Limited cross-bed orientations imply onshore paleowinds from the SSE (160°). The aeolianite may signal a fall in sea level leading into the Ghaub glaciation, analogous to Quaternary calcareous aeolianites rimming modern carbonate platforms [*Brooke*, 2001]. We do not know if the apparent uniform $\delta^{13}C$ values near −2.5‰ represent the composition of the last carbonate to be deposited before the sea level fall or a mixture of grains from different stratigraphic levels exposed by erosion.

3.6. Southern Foreslope

[25] Deepwater rhythmites and grain flows comprising the foreslope facies (MS 17–18) have variable but exclusively negative $\delta^{13}C$ values between 0 and −4‰ (Figure 8). The absence of any positive values is surprising given our expect-

ation that slope strata equivalent to cycles 1–6 on the shelf would be present. An obvious explanation would be a ~7‰ lower $\delta^{13}C$ in the water column at depth [namely *Groztinger and Knoll*, 1995; *Calver*, 2000], but we hesitate to draw this inference because the slope deposits are allodapic (Figure 3c) and originated in shallower water. Alternatively, slope deposits equivalent to cycles 1–6 might be subsumed within the underlying mixed carbonate-siliciclastic turbidites assigned to the Gruis Formation (Figure 2), were never deposited because the sampled slope sections represent zones of sediment bypass, or were deposited and subsequently removed by submarine erosion (landsliding) before deposition of the sampled rhythmites and grainflows. Both the latter alternatives fit with the inference, based on erosional truncation of the upper Ombaatjie on the inner shelf (Figure 6), that sea level fell prior to glaciation of the platform. We tentatively interpret the Ombaatjie foreslope deposits as a type 1

lowstand wedge [*Sarg*, 1988] associated with this sea level fall. They could be broadly equivalent in age to the aeolianite (MS 14) at the shelf edge and erosion elsewhere on the shelf. We cannot rule out the alternative that the slope deposits are correlative with cycles 7–8, but we consider a reciprocal relationship between shelf and slope sedimentation to be more realistic.

4. Timescale of the Preglacial $\delta^{13}C$ Anomaly

[26] In order to evaluate alternative mechanisms for the upper Ombaatjie isotopic shift, the rate of $\delta^{13}C$ change with time is crucial. Unfortunately, the duration of this ancient isotopic shift cannot be estimated by radiometric or magnetostratigraphic means. However, given that the shift occupies at least one complete depositional cycle, beginning and ending at sea level, and that no significant postdepositional compaction has occurred, we could estimate the duration of the shift from its stratigraphic thickness (20–50 m) if we knew the background tectonic subsidence rate, assuming no large, net, change in sea level.

[27] To this end, we use a simple, one-dimensional, thermal subsidence model of the *McKenzie* [1978] type to estimate long-term sediment accumulation rates [*Hoffman et al.*, 1998a; *Halverson et al.*, 1998]. In order to construct the model, we must estimate the total passive-margin sediment thickness (L_{tot}) and the duration of sedimentation (t_{tot}). Correcting L_{tot} for the isostatic effect of sediment loading, a uniform crustal stretching factor (β) can be determined graphically [*McKenzie*, 1978]. Using this β factor, tectonic subsidence can be calculated as a function of time using the heat flow equation [*McKenzie*, 1978]. We can apply the inverse problem and back calculate a duration of sedimentation from sediment thickness (L_s) if we employ a series of simplifying assumptions: (1) no net sea level change, (2) no net change in water depth, (3) insignificant compaction, (4) uniform (carbonate) sediment density of 2.65 g cm^{-3}, and (5) no isostatic effects from erosion. These are all justifiable assumptions, given our knowledge of the regional stratigraphic context (Figures 6, 7, and 8). Because

L_s decreases exponentially as a funciton of time, a time period (t_1) since the onset of thermal subsidence (t_0) must be also be assumed. However, by simplifying $t_1 = t_0$, the minimum time required ($t_2 - t_1$) for deposition of a given L_s is calculated (i.e., assuming the initial, most rapid, thermal subsidence rate).

[28] As discussed earlier, stratigraphic relationships indicate that rifting effectively ceased on the Huab and Makalani ridges during the Gruis-Ombaatjie transition (Figure 2), although the Makalani ridge was slightly reactivated in Ghaub times. Thus the passive-margin sediments include the Ombaatjie Formation and the Tsumeb Subgroup (Figure 2). In the study area (Figure 1), these sediments are 1.5 km thick. However, 400 km to the east, in the Otavi Mountains, they are much thicker [*Hedberg*, 1979; *Miller*, 1997]. Unpublished $\delta^{13}C$ data demonstrate that there is ~1.0 km of additional strata younger than any in the study area. For the purposes of this model, we prescribe a window for L_{tot} of 1.5–2.5 km.

[29] The duration of passive-margin sedimentation (t_{tot}) is poorly constrained. The maximum duration is ~120 my, as sedimentation began after 746 Ma (Ombombo subgroup volcanics, *Hoffman et al.*, 1996) and ended when the Otavi margin collided with the Rio Plata craton ~630 Ma [*Alkmim et al.*, 2001]. If t_{tot} was less than half this amount (<60 × 10^6 years), unreasonably large β factors are implied, inconsistent with the degree of extension observed on the Makalani and Huab ridges. We therefore calculate a window between 60 and 120 × 10^6 years for t_{tot}.

[30] Notwithstanding the wide t_{tot} and L_s window, β is constrained to between 1.35 and 1.12 (Figure 9a). In applying the model to the timescale of the upper Ombaatjie $\delta^{13}C$ shift, we calculate the minimum time (t_s) it took to deposit cycle 7, which encompasses nearly the entire $\delta^{13}C$ shift. Cycle 7 ranges generally between 32 and 48 m in thickness (Figures 6, 7, and 8), and we plot these bounds as a function of β (Figure 9b). For $\beta =$ 1.20 (which falls in the middle of the window in Figure 9a), t_s is estimated to be 0.50–0.75 × 10^6 years (Figure 9b). Note that t_s is relatively insen-
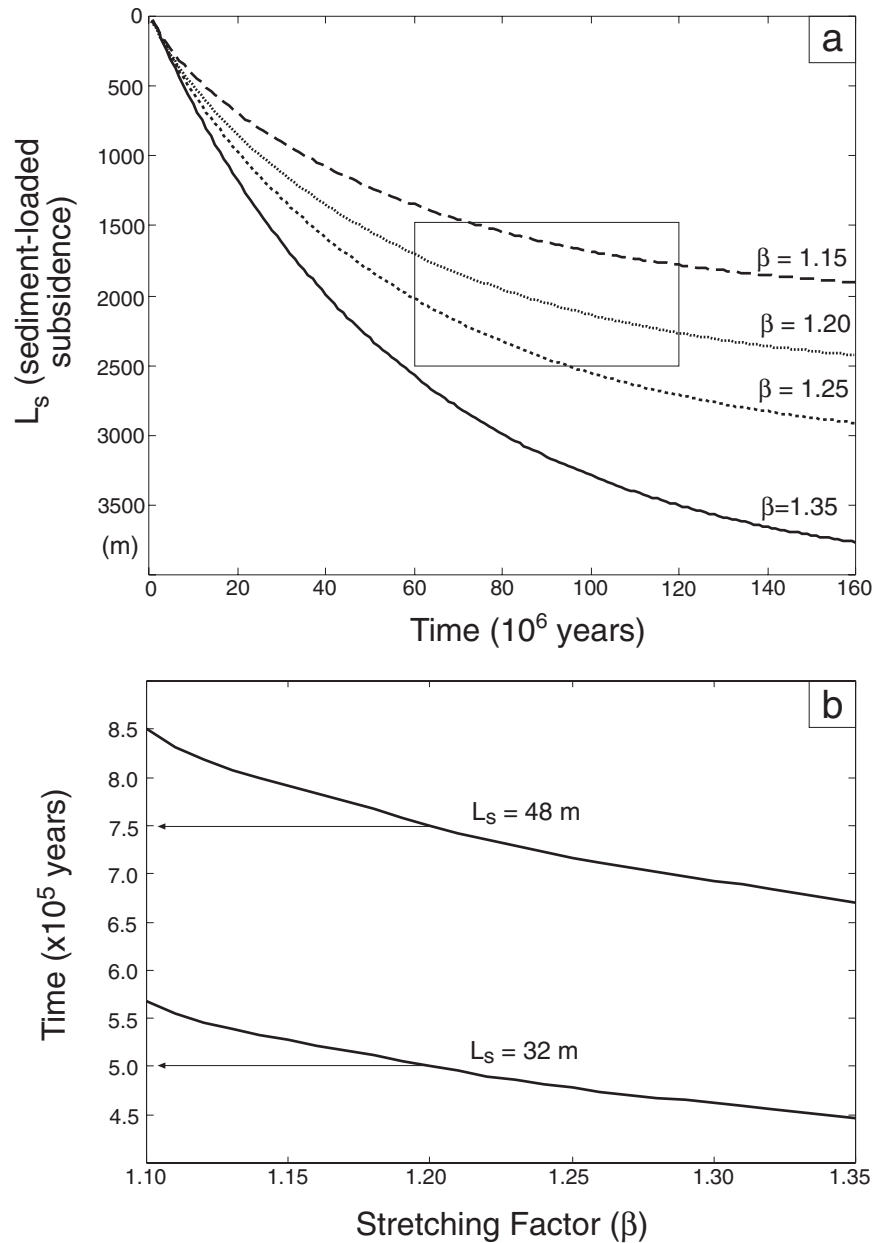
Figure 9. (a) Thermal subsidence model based on *McKenzie* [1978] in which L_s, total sediment-loaded subsidence (thermal subsidence plus isostatic compensation due to sediment loading), is plotted as a function of time for variable stretching factors (β). The box represents the window of our estimate for the total thickness of Otavi passive margin sediments (1500 to 25000 m) and time span (between 60 and 120×10^6 yeras) over which these sediments were deposited. Both of these parameters are required for estimating β. (b) Plot of time required for deposition of a given thickness of sediments, L_s, (calculated by assuming that the tectonic subsidence rate can be approximated as linear, which is appropriate for this short timescale) as a function of β (varied from 1.10 to 1.35 as per the window in Figure 9a). The two curves correspond to $L_s = 32$ and 48 m, the bounds on the stratigraphic thickness of cycle 7 in Huab dip slope sections (MS14−16). Arrows point to upper and lower time constraints ($0.5-7.5 \times 10^6$ years) for duration of deposition of cycle 7, assuming a β = 1.20. This same model is used to calculate an approximate sedimentation rate or 65 m/10^6 yr^{-1} for the Ombaatjie as a whole.

sitive to changes in β (varying by ~0.15 × 10⁶ years over the range in β) and that the greatest source of uncertainty is L_s. As the upper Ombaatjie isotopic shift occurred soon after the rift-drift transition, this estimate for t_s, while strictly a minimum bound, may be a reasonable approximation of its true duration as the subsidence rate should not have changed greatly over the time span of the Ombaatjie Formation (Figure 9a). For convenience, we can idealize the result by inferring a mean, linear sedimentation rate for the Ombaatjie Formation of roughly 65 m/10⁶ yr⁻¹. This rate yields a minimum of 0.9 × 10⁶ years between the beginning of the δ¹³C deviation and the onset of sea level fall associated with the Ghaub glaciation and a duration of at least 3 × 10⁶ years for deposition of the entire Ombaatjie Formation.

5. Is the Preglacial δ¹³C Anomaly Global?

[31] The concordance of the isotopic shift with the cyclic stratigraphy and the discordance of the glacial erosion surface (Figures 6, 7, and 8) argue against a diagenetic origin for the anomaly, as suggested by *Kennedy et al.* [2001a]. However, even if the δ¹³C values are primary and closely represent seawater over the Otavi platform, does the preglacial anomaly represent a global event? We begin this inquiry by comparing isotopic profiles from the inner and outer parts of the Otavi shelf (Figure 10), including sections (MS 14 and 16) within 10 km of the shelf break (Figure 1). In Figure 10, data from all 16 shelf sections (Figures 6, 7, and 8) were individually normalized to the regional mean thicknesses of cycles 3–6, 7 and 8, and then collectively stacked. The vertical scale is time, based on the estimated long-term accumulation rate of 65 m/10⁶ yr⁻¹. Most striking in this figure is the coherence of the secular decline in δ¹³C in cycle 7, the estimated duration of which is ~0.6 × 10⁶ years. The greater scatter in data for cycle 8 is partly an artifact of thickness normalization because of the variable preservation of this cycle beneath the glacial disconformity. Although the slope of the isotopic shift is remarkably similar on the inner and outer shelf (Figure 10), its ampli-

tude is somewhat larger (~12‰) in the more restricted setting. The shift of 8–11‰ on the outer shelf should more closely approximate the global signal.

[32] The preglacial negative anomaly is not unique to Namibia: analogous δ¹³C shifts of equal or greater magnitude occur in the Trezona Formation beneath the Elatina glaciation in South Australia [*McKirdy et al.*, 2001; *Walter et al.*, 2000], in the upper Keele Formation below the Ice Brook glaciation in the northern Canadian Cordillera [*Narbonne et al.*, 1994; *Kaufman et al.*, 1997; *Hoffman and Schrag*, 2002], and in the upper Yukkengol Formation beneath the Hankalchoug glaciation of the central Tien Shan in northwest China [*Xiao et al.*, 2001]. The negative anomaly bottoms out at −9‰ (PDB) in Australia, −7‰ in Canada, and −11‰ in China. All three represent the younger of two Neoproterozoic glaciations in their respective regions and are thought to be correlative for other reasons [*Brookfield*, 1994; *Kennedy et al.*, 1998; *Walter et al.*, 2000].

[33] More fragmentary data suggest that similar preglacial anomalies occur in the Elbobreen Formation in Svalbard [*Fairchild and Spiro*, 1987; *Kaufman et al.*, 1997; *Halverson and Maloof*, 2001] and in the Lossit Limestone beneath the Port Askaig Tillite in Scotland [*Brasier and Shields*, 2000]. These two precede the older of two glaciations in their respective regions and could represent a separate event [*Kennedy et al.*, 1998; *Prave*, 1999; *Brasier and Shields*, 2000; *Condon and Prave*, 2000], but in no single region are two preglacial anomalies known. In Namibia, crustal block rotation and erosion coincident with the older Chuos glaciation (Figure 2) has removed much of the preglacial stratigraphic record. Nevertheless, the existence of similarly large preglacial anomalies in five far-flung regions suggests that they are global and that their connection to glaciation is not fortuitous.

6. Origin of the Preglacial δ¹³C Anomaly

[34] There are many mechanisms, operating alone or in combination, by which δ¹³C variation in
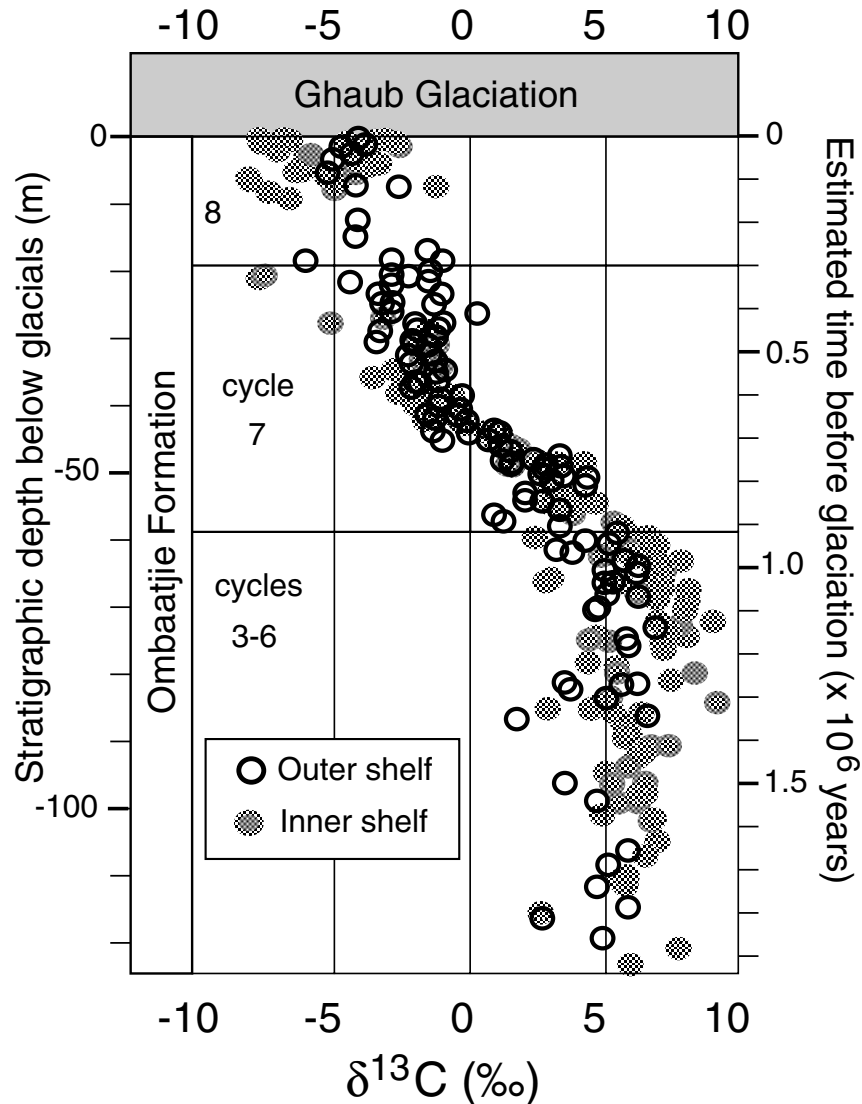
Figure 10. Composite $\delta^{13}C$ record through Ombaatjie cycles 3–8 from inner and outer shelf sections (MS1-16). The composite was constructed by normalizing cycles 3–6, 7, and 8 independently to mean thickness for each section and then stacking the $\delta^{13}C$ data from all the sections. Note that the $\delta^{13}C$ deviation in cycle 7 is very coherent and that the amplitude of the $\delta^{13}C$ deviation in Hoanib shelf and Makalani dip slope (inner shelf) is greater than on the Huab dip slope (outer shelf) by ~4‰. Scatter is likely a result of (1) variability of sediment accumulation rates between sections, (2) erosion on sequence boundaries, particularly atop cycle 8, (3) and inclusion of questionable data from sheared and marly limestones. Timescale on the right is based on a 65 m/10^6 yr^{-1} sediment accumulation rate derived from our thermal subsidence model (Figure 9).

seawater might occur. Many of these mechanisms have been reviewed, in particular with respect to Phanerozoic $\delta^{13}C$ variations on the order of a few per mil [e.g., *Kump*, 1991; *Kump and Arthur*, 1999]. A variety of explanations have also been invoked to explain the much larger anomalies characteristic of the Neoproterozoic [*Kaufman and Knoll*, 1995; *Hoffman et al.*, 1998a; *Kennedy*

et al., 2001b]. However, as detailed documentation of a preglacial anomaly is only now emerging, its cause is poorly understood. Here we briefly discuss several conventional mechanisms as they might pertain to the Ombaatjie $\delta^{13}C$ record, specifically judging whether they can account for both the geological context of the isotopic shift and its inferred duration.

[35] The timescale we infer for the isotopic shift ($\sim 0.6 \times 10^6$ years) is greater than the residence time of carbon in the oceans (~ 150 kyr), which means that we should assume a steady state between the major inputs and outputs of carbon with respect to the oceanic-atmospheric system. Inputs are volcanic and metamorphic outgassing of CO_2 and oxidation of reduced carbon species such as organic matter (OM) and methane (CH_4). Outputs are marine sedimentary carbonate and OM. The isotopic composition of the ocean as a whole is governed by the $\delta^{13}C$ of total input ($\delta^{13}C_{input}$) and by the fraction of organic carbon to total carbon burial (f_{org} = OM burial/C burial [*Holland*, 1984; *Summons and Hayes*, 1992]). The $\delta^{13}C$ of carbonate and OM derived from the surface ocean can be further modified by a surface-to-deep negative $\delta^{13}C$ gradient maintained by the biological "pump" [*Broecker and Peng*, 1982]. A change in the $\delta^{13}C$ of marine carbonates with time could result from a change in $\delta^{13}C$ of the input or output of carbon or a change in isotopic fractionation between the various reservoirs within the ocean-atmosphere system.

6.1. Lowered Organic Productivity

[36] Negative $\delta^{13}C$ excursions in certain Phanerozoic marine carbonates are inferred to record dramatic declines in primary productivity [e.g., *Hsü et al.*, 1985; *Zachos et al.*, 1989; *D'Hondt et al.*, 1998; *Jin et al.*, 2000; *Ward et al.*, 2001], which lower f_{org}. Similarly, *Hoffman et al.* [1998a] tentatively attributed the upper Ombaatjie shift to a collapse in biological productivity as the Ghuab glaciation intensified but before it had reached the latitude of the Otavi margin. A reduction in f_{org} to near 0 would cause the $\delta^{13}C$ of the whole ocean to evolve toward $\delta^{13}C_{input}$, assumed to be approximately $-5‰$ for the Neoproterozoic [*Hayes et al.*, 1999]. The rate at which $\delta^{13}C$ evolves is controlled by the residence time of C in the ocean. Following a complete cessation of OM burial, $\delta^{13}C$ would decline exponentially, approaching $\delta^{13}C_{input}$ at $\sim 0.5 \times 10^6$ years [*Kump*, 1991].

[37] This timescale is consistent with the upper Ombaatjie $\delta^{13}C$ shift, yet several lines of reasoning argue against a sudden drop in productivity, assum-

ing such a biological catastrophe would be driven by nutrient limitation. First, a near-total collapse in productivity is unlikely so long as the tropical ocean (e.g., the Otavi shelf) remains open. As already noted, the onset of the Ombaatjie $\delta^{13}C$ decline predates any significant sea level fall (beginning at least 0.9×10^6 years before the onset of continental glaciation), so glaciation cannot be invoked as limiting riverine and wind-born nutrient supply. Nor can sea ice cover in the high latitudes be responsible for dramatically lowering f_{org} as this would drive nutrient upwelling to the lower latitudes. As Neoproterozoic continents were clustered in the low-latitudes [*Kirschvink*, 1992b; *Kent and Smethurst*, 1998], primary production would have been focused closer to continental margins where OM burial is most likely to occur [*Hedges and Keil*, 1995]. Moreover, a dramatic lowering of OM burial would lead to increased nutrient availability, driving higher productivity (a negative feedback), unless accompanied by a lowered C:P of the OM burial flux. Sudden ventilation of previously anoxic deep waters or restricted basins could simultaneously lower the OM burial flux and its C:P ratio [*Van Cappellen and Ingall*, 1994], but it should not cause f_{org} to drop far below the present value of ~ 0.2, which represents a highly ventilated state of the ocean.

[38] It could be argued that pCO_2 declined sufficiently during the period of prolific OM burial (signaled by the high $\delta^{13}C$ prior to the negative shift) to cause a loss of productivity by CO_2 limitation [*Riebesell et al.*, 1993] and a decline in the isotopic fractionation between DIC and OM [*Bidigare et al.*, 1997; *Kump and Arthur*, 1999], both of which would lower $\delta^{13}C$. However, productivity decline as a function of pCO_2 should be a self-limiting process incapable of effecting a dramatic perturbation in the global carbon cycle. Furthermore, a catastrophic decline in productivity would eliminate a major sink for atmospheric CO_2. A resulting CO_2 buildup contradicts impending glaciation, unless it is compensated for by the albedo effect of sea ice. Presumably combined low pCO_2 and polar sea ice cover would destabilize the climate and drive rapid global glaciation (~ 2000 years [*Hyde et al.*, 2000]), which is

inconsistent with our assumed timescale for the Ombaatjie shift.

6.2. Ocean Overturn

[39] Abrupt changes in the oceans' overturning circulation have been invoked to explain the Neoproterozoic marine $\delta^{13}C$ record [*Kaufman et al.*, 1991; *Groztinger and Knoll*, 1995; *Hill and Walter*, 2000]. In this model, a low rate of overturn is inferred for the nonglacial periods whereby OM is sequestered in a stagnant deep ocean, driving $\delta^{13}C$ in surface waters to the unusually high values characteristic of nonglacial periods. The result is a large surface-to-deep $\delta^{13}C$ gradient. Drawdown of atmospheric CO_2 eventually leads to glaciation, which in turn enhances thermohaline overturning. Overturn causes the ^{13}C-depleted, DIC-charged, deep water to invade the surface, releasing CO_2 to the atmosphere (initiating deglaciation) and precipitating carbonates with low $\delta^{13}C$.

[40] Ocean overturn amounts to a rapid mixing of the surface and deep ocean reservoirs. Assuming that stagnation is physically possible for periods exceeding the carbon residence time (~150 kyr) and also that productivity could be maintained in surface waters if the nutrient flux from depth was curtailed, the deep ocean DIC could evolve to negative $\delta^{13}C$ values, while the surface ocean would be highly enriched in ^{13}C [*Groztinger and Knoll*, 1995]. As the deep ocean reservoir dwarfs the surface ocean, mixing of the two should cause an isotopic shift in surface water on a decadal timescale [*Kump*, 1991]. The upper Ombaatjie $\delta^{13}C$ shift was not rapid, however, but declined gradually over 100s of kyr.

6.3. Preferentially Enhanced Weathering of Organic Matter

[41] Another way to drive a negative $\delta^{13}C$ excursion is to increase the contribution of weathered OM to total carbon input to the oceans. One way this could be achieved is tectonic uplift of black shale [e.g., *Derry and France-Lanord*, 1996; *Petsch and Berner*, 1998]. This may be a viable mechanism for shifts on the order of 1-3‰, but it seems unlikely that OM weathering could ever so

dominate the input budget as to drive $\delta^{13}C_{input}$ to -15‰, as required for an 11‰ shift (assuming constant f_{org}). Alternatively, several authors [*Berger and Vincent*, 1986; *Magaritz et al.*, 1988; *Kaufman et al.*, 1991] have proposed that a drop in sea level might expose organic-rich shelf sediments to weathering. This mechanism requires that shelf sediments have a higher proportion of OM to carbonate on average than sediments in the ocean as a whole. However, this seems unlikely before the Mesozoic-Cenozoic, when significant carbonate began to be sequestered in deep water due to the rise of calcareous nanoplankton [*Wilkinson and Walker*, 1989]. In the Neoproterozoic, when most carbonate was deposited in shallow water, large changes in the ratio of OM to carbonate in the weathering flux would have been difficult to achieve through changes in sea level alone. Moreover, a drop in sea level could not have exceeded the tectonic subsidence rate for there to be a stratigraphic record of the isotopic shift on the Otavi shelf, which would otherwise have been exposed.

6.4. Methane Release

[42] The potency of methane as a greenhouse gas (~30 times that of CO_2, molecule for molecule) and its highly ^{13}C-depleted isotopic composition ($\delta^{13}C \approx -60$‰ [*Kvenvolden*, 1993]) make it a popular candidate to explain $\delta^{13}C$ excursions that appear temporally correlated to rapid global warming events. Modern continental margins store vast quantities ($\sim10,000$ Gt [*Kvenvolden*, 1993]) of methane hydrates. Gas hydrate stability is a function of pressure, temperature, water activity, and gas composition [*Buffet*, 2000; *Dickens*, 2001]. Several processes can potentially cause gas-hydrate dissociation and methane release into the oceans (and subsequently the atmosphere if the water column is anoxic or the release is very rapid). Release mechanisms include slope failure, sea level fall, and increase in either bottom water temperatures or the geothermal gradient [*Kvenvolden*, 1993]. Release of a large volume of methane to the atmosphere would increase the global greenhouse forcing and cause a decline in marine $\delta^{13}C$ as the isotopically light carbon propagated through the carbon cycle.

[43] A catastrophic methane release is the probable cause of the Late Paleocene Thermal Maximum and the associated $\delta^{13}C$ excursion seen in both terrestrial [*Koch et al.*, 1992] and marine records [*Dickens et al.*, 1995; *Katz et al.*, 1999]. Gas hydrate dissociation has been implicated in various other perturbations in the global carbon cycle and climate, including Quaternary interstadials [*Kennet et al.*, 2000], an Early Cretaceous $\delta^{13}C$ excursion [*Jahren et al.*, 2001], two separate Jurassic events [*Hesselbo et al.*, 2000; *Padden et al.*, 2001], and the Permo-Triassic boundary [*Krull and Retallack*, 2000]. In all these cases, the shift in $\delta^{13}C$ is only $\sim$2‰. Assuming methane hydrate $\delta^{13}C \approx -60$‰ [*Kvenvolden*, 1993] and a DIC mass of $\sim$38,000 Gt [*Falkowski et al.*, 2000], 9600 Gt of methane is required to drive a rapid, whole-ocean, isotopic shift of 11‰. A single methane burst of this magnitude seems implausible given the required mass is approximately equal to the total estimated present-day methane hydrate reservoir [*Kvenvolden*, 1993; *Dickens*, 2001]. A more likely explanation would be an anomalous methane flux that was sustained for 100s kyr, consistent with the gradual nature of the isotopic shift in the Ombaatjie Formation. The total mass of methane required to drive the $\delta^{13}C$ decline in this case would exceed 9600 Gt but is highly uncertain and dependent on the timescale.

[44] *Pavlov et al.* [2000] hypothesized that oxidation of the atmosphere $\sim$2.4 Ga eliminated the methane component of the Earth's early greenhouse, giving rise to the first widespread glaciations [*Evans et al.*, 1997; *Williams and Schmidt*, 1997; *Schmidt and Williams*, 1999; *Kirschvink et al.*, 2000]. In related arguments, both *Schrag et al.* [2002] and *Pavlov et al.* [2001] have proposed a methane trigger for Neoproterozoic snowball glaciation. According to the *Schrag et al.* [2002] hypothesis, a high methane flux from anoxic tropical basins sustained for 100s kyr could account for the preglacial $\delta^{13}C$ shift. The consequent global warming and increased silicate weathering would draw down CO_2, leading to a critical dependence on greenhouse methane. Because atmospheric methane concentration is not buffered by the ocean, as is CO_2 and because of its short

residence time, any short-term interruption in the methane flux could cause a catastrophic loss of greenhouse forcing, plunging the Earth into an ice age.

[45] This model requires one mechanism to increase the methane flux to the atmosphere, accounting for the $\delta^{13}C$ decline and another to decrease it (leading to glaciation). Another requirement of this model is that the methane that is released must have originally been sequestered and stored separate from the isotopically enriched CO_2 also produced during methanogenesis. The large reservoir of methane stored as a clathrate in highly productive tropical basins [*Schrag et al.*, 2002] is the most likely candidate. *Schrag et al.* [2002] tentatively postulate that one mechanism which would be consistent with the inferred timescale of the $\delta^{13}C$ shift and could account for both the onset and cessation of the methane flux would be the tectonic uplift of a clathrate-rich basin. In this scenario, the elevated methane flux would naturally cease after the clathrate reservoir was depleted.

[46] *Pavlov et al.* [2001] argue that a highly nonlinear relationship between marine sulfate concentration and the atmospheric mixing ratio of methane may have been responsible for rapid changes in the greenhouse forcing of the atmosphere. Whereas this relationship may have been important in modulating methane fluxes, it cannot alone explain the shift in $\delta^{13}C$ and requires a separate mechanism to modify sulfate concentrations. Thus both methane trigger hypotheses remains speculative at present. Nonetheless, the potency of methane in regulating climate and $\delta^{13}C$ makes it a likely culprit in both the preglacial isotopic anomaly and the subsequent ice age.

7. Conclusions

[47] The $\delta^{13}C$ of lithologically unremarkable shelf carbonates declines smoothly by >10‰ over an estimated time span of $\sim$0.6 $\times$ 10^6 years in advance of the Neoproterozoic glacial event in Namibia previously ascribed to a snowball Earth [*Hoffman et al.*, 1998a]. The decline follows a much longer period (>10^7 years) during which

δ^{13}C values were consistently greater than +5‰ (PDB). The coherence of the isotopic shift in 16 sections (Figure 10) across the ancient shelf and its relation to the succeeding glacial erosion surface, indicate that the anomaly is primary and records a major perturbation of the global carbon cycle. The δ^{13}C decline began well in advance (>0.9 × 10^6 years) of the sea level fall associated with glaciation. Given evidence that the glaciation was long-lived [*Hoffman et al.*, 1998a], the preglacial δ^{13}C anomaly must be distinct from that observed in the postglacial cap-carbonate sequence (Maieberg Formation) and should have originated independently. Similar preglacial anomalies are observed in the Neoproterozoic in Australia, Canada, China, Scotland, and Svalbard, which suggests that the connection to glaciation is not fortuitous.

[48] The estimated timescale and geological context make the preglacial anomaly difficult to reconcile with conventional explanations; lowered organic productivity, ocean overturn, enhanced organic weathering, or a massive methane burst. An alternative hypothesis involves a prolonged methane release, engendered by organic-rich sediments in anoxic basins on continental margins then disproportionally disposed in the tropics [*Schrag et al.*, 2002]. This idea is consistent with the high δ^{13}C values (greater than +5‰ PDB) that precede the negative shift in Namibia and elsewhere [*Kaufman et al.*, 1997; *Walter et al.*, 2000]. Counterintuitively, a high methane flux sustained for 100s kyr would not be incompatible with glaciation and might even be the agent of climatic destabilization that led to the snowball Earth [*Schrag et al.*, 2002]. Furthermore, this model predicts a transient period of global warming accompanying the initial rise of atmospheric methane (before consequent CO_2 lowering), which might be detectable in the stratigraphic record.

Acknowledgments

References

Alkmim, F. F., S. Marshak, and M. A. Fonseca, Assembling West Gondwana in the Neoproterozoic: Clues from the São Fransicso craton region, Brazil, *Geology*, 29, 319–322, 2001.

Banner, J. L., and G. N. Hanson, Calculation of simultaneous isotopic and trace element variations during water-rock interaction with applications to carbonate diagenesis, *Geochim. Cosmochim. Acta*, 54, 3123–3137, 1990.

Berger, W. H., and E. Vincent, Deep-sea carbonates: Reading the carbon-isotope signal, *Geol. Rundsch.*, 75, 249–269, 1986.

Bidigare, R. R., et al., Consistent fractionation of ^{13}C in nature and in the laboratory: growth rate effects in some haptophyte algae, *Global. Biogeochem. Cycles*, 11, 279–292, 1997.

Brand, U., and J. Veizer, Chemical diagenesis of a multicomponent carbonate system −2: Stable isotopes, *J. Sediment. Petrol.*, 51, 987–997, 1981.

Brasier, M. D., and G. Shields, Neoproterozoic chemostratigraphy and correlation of the Port Askaig glaciation, Dalradian Supergroup of Scotland, *J. Geol. Soc.*, 157, 909–914, 2000.

Broecker, W. S. , and T.-H. Peng, *Tracers in the Sea*, 690 pp., Lamong-Doherty Earth Observatory, Palisades, N.Y., 1982.

Brooke, B., The distribution of carbonate eolianite, *Earth Sci. Rev.*, 55, 135–164, 2001.

Brookfield, M. E., Problems in applying preservation, facies and sequence models to Sinian (Neoproterozoic) glacial sequences in Australia and Asia, *Precambrian Res.*, 70, 113–143, 1994.

Buffet, B., Clathrate hydrates, *Ann. Rev. Earth Planet. Sci.*, 28, 477–507, 2000.

Calver, C. R., Isotope Stratigraphy of the Ediacaran (Neoproterozoic III) of the Adelaide rift complex, Australia, and the overprint of water column stratification, *Precambrian Res.*, 100, 299–312, 2000.

Clauer, N., and A. Kröner, Strontium and argon isotopic homogenization of pelitic sediments during low-grade regional metamorphism: the Pan-African upper Damara sequence of northern Namibia, *Earth Planet. Sci. Lett.*, 43, 117–131, 1979.

Condon, D. J., and A. R. Prave, Two from Donegal: Neoproterozoic glacial episodes on the northeast margin of Laurentia, *Geology*, 28, 951–954, 2000.

Craig, H., Isotopic standards for carbon and oxygen and correction factors for mass-spectrometric analysis of carbon dioxide, *Geochim. Cosmochim. Acta*, 12, 133–149, 1957.

Derry, L. A., and C. France-Lanord, Neogene growth of the sedimentary organic carbon reservoir, *Paleoceanography*, 11, 267–275, 1996.

Derry, L. A., A. J. Kaufman, and S. E. Jacobsen, Sedimentary cycling and environmental change in the late Proterozoic: Evidence from stable and radiogenic isotopes, *Geochim. Cosmochim. Acta*, *56*, 1317–1329, 1992.

D'Hondt, S., P. Donaghay, J. C. Zachos, D. Luttenberg, and M. Lindinger, Organic carbon fluxes and ecological recovery from the Cretaceous-Tertiary mass extinction, *Science*, *282*, 276–279, 1998.

Dickens, G. R., Modeling the global carbon cycle with a gas hydrate capictor: Significance for the Latest Paleocene thermal maximum, in *Natural Gas Hydrates: Occurrence, Distribution, and Detection, Geophys. Monogr. Ser.*, vol. 124, edited by C. K. Paull and W. P. Dillon, pp. 19–38, AGU, Washington D.C., 2001.

Dickens, G. R., J. R. O'Neil, D. K. Rea, and R. M. Owen, Discussion of oceanic methane hydrate as a cause of the carbon isotope excursion at the end of the Paleocene, *Paleoceanography*, *10*, 965–971, 1995.

Dürr, S. B., and D. P. Dingeldey, Tale of three cratons: Tectonostratigraphic anatomy of the Damada orogen in northwestern Namibia and the assembly of Gondwana: Comment, *Geology*, *25*, 1149–1150, 1997.

Evans, D. A., Stratigraphic, geochronological, and paleomagnetic constraints upon the Neoproterozoic climatic paradox, *Am. J. Sci.*, *300*, 347–433, 2000.

Evans, D. A., N. J. Beukes, and J. L. Kirschvink, Low-latitude glaciation in the Palaeoproterozoic, *Nature*, *386*, 262–266, 1997.

Fairchild, I. J., and B. Spiro, Petrological and isotopic implications of some contrasting Late Precambrian carbonates, NE Spitsbergen, *Sedimentology*, *34*, 973–989, 1987.

Falkowski, P., et al., The global carbon cycle: A test of our knowledge of Earth as a system, *Science*, *290*, 291–296, 2000.

Frets, D. C., Geology and Structure of the Huab-Welwitschia Area, South West Africa, Bulletin Precambrian Research Unit, *5*, 235 pp., Univ. of Cape Town, Rondebosch, South Africa, 1969.

Groztinger, J. P., and A. H. Knoll, Anomalous carbonate precipitates: Is the Precambrian the key to the Permian, *Palaios*, *10*, 578–596, 1995.

Guj, P., The Damara mobile belt in south-western Kaokoveld, South West Africa, Bulletin Precambrian Research Unit, *8*, 168 pp., Univ. of Cape Town, Rondebosch, South Africa, 1970.

Halverson, G. P., and A. C. Maloof, Getting into global glaciation (abstract), paper presented at European Union of Geosciences, Strasbourg, Fr., 2001.

Halverson, G. P., P. F. Hoffman, and A. J. Kaufman, Numerically constraining the duration of Neoproterozoic carbon isotope excursions (abstract), *Geol. Soc. Am. Abstr. Programs*, *30*, 221, 1998.

Hambrey, M. J., and W. B. Harland, *Earth's Pre-Plestocene Glacial Record*, 1004 pp., Cambridge Univ. Press, New York, 1981.

Hayes, J. M., H. Strauss, and A. J. Kaufman, The abundance of ^{13}C in marine organic matter and isotopic fractionation in the global biogeochemical cycle of carbon during the past 800 Ma, *Chem. Geol.*, *161*, 103–126, 1999.

Hedberg, R. M., Stratigraphy of the Ovamboland Basin, Southwest Africa, Bulletin Precambrian Research Unit, *24*, 325 pp., Univ. of Capetown, Rondebosch, South Africa, 1979.

Hedges, J. I., and R. G. Keil, Sedimetnary organic matter preservation: an assessment and speculative synthesis, *Mar. Chem.*, *49*, 81–115, 1995.

Henry, G., C. W. Clendenin, I. G. Stanistreet, and K. J. Malden, A multiple detachment model for the early rifting stage of the Late Proterozoic Damara Orogen in Namibia, *Geology*, *18*, 67–71, 1990.

Hesselbo, S. P., D. R. Gröcke, J. C. Jenkyns, C. J. Bjerrum, P. Farrimond, H. S. Morans Bell, and O. R. Green, Massive dissociation of gas hydrate during a Jurassic oceanic anoxic event, *Nature*, *406*, 392–395, 2000.

Hill, A. C., and M. R. Walter, Mid-Neoproterozoic (~830–750 Ma) isotope stratigraphy of Australia and global correlation, *Precambrian Res.*, *100*, 181–211, 2000.

Hoffmann, K.-H., and A. R. Prave, A preliminary note on a revised subdivision and regional correlation of the Otavi Group based on glaciogenic diamictites and associated cap dolostones, *Communs. Geol. Soc. Namibia*, *11*, 81–86, 1996.

Hoffman, P. F., Is the coincidence of Neoproterozoic glacial deposits with unconformities compatible with the "snowball earth" hypothesis? (abstract), paper presented at the Annual Meeting of Geological Society of America, Reno, Nev., 2000.

Hoffman, P. F., and E. H. Hartz, Large, coherent, submarine landslide associated with Pan-African foreland flexure, *Geology*, *27*, 687–690, 1999.

Hoffmann, P. F., and D. P. Schrag, The snowball Earth hypothesis: Testing the limits of global change, *Terra Nova*, in press, 2002.

Hoffman, P. F., D. P. Hawkins, C. E. Isachsen, and S. A. Bowring, Precise U-Pb zircon ages for early Damaran magmatism in the Summas Mountains and Welwitschia Inlier, northern Damara belt, Namibia, *Communs. Geol. Surv. Namibia*, *11*, 47–52, 1996.

Hoffman, P. F., A. J. Kaufman, G. P. Halverson, and D. P. Schrag, A Neoproterozoic snowball Earth, *Science*, *281*, 1342–1346, 1998a.

Hoffman, P. F., A. J. Kaufman, and G. P. Halverson, Comings and goings of global glaciations on a Neoproterozoic tropical platform, *GSA Today*, *8*, 1–9, 1998b.

Hoffman, P. F., G. P. Halverson, and J. P. Grotzinger, Are Proterozoic cap carbonates and isotopic excursions a record of gas hydrate destabilization following Earth's coldest intervals?: Comment, *Geology*, *30*, 286–287, 2002.

Holland, H., *The Chemical Evolution of the Atmosphere and Oceans*, 582 pp., Princeton Univ. Press, Princeton, N.J., 1984.

Hsü, K. J., H. Oberhänsli, J. Y. Gao, S. Shu, C. Haihong, and Y. Krähenbühl, "Strangelove ocean" before the Cambrian explosion, *Nature*, *316*, 809–811, 1985.

Hyde, W. T., T. J. Crowley, S. K. Baum, and W. R. Peltier, Neoproterozoic "snowball Earth" simulations with a coupled climate/ice-sheet model, *Nature*, *405*, 425–429, 2000.

Irwin, H., C. Curtis, and M. Coleman, Isotopic evidence for source of diagenetic carbonates formed during burial of organic-rich sediments, *Nature*, *269*, 209–213, 1977.

Jahren, A. H., N. C. Arens, G. Sarmiento, J. Guerrero, and R. Amundson, Terrestrial record of methane hydrate dissociation in the Early Cretaceous, *Geology*, *29*, 159–162, 2001.

Jin, Y. G., Y. Wang, W. Wang, Q. H. Shang, C. Q. Cao, and D. H. Erwin, Pattern of marine mass extinction near the Permian-Triassic boundary in South China, *Science*, *289*, 432–436, 2000.

Katz, M. E., D. K. Pak, G. R. Dickens, and K. G. Miller, The source and fate of massive carbon input during the latest Paleocene thermal maximum, *Science*, *286*, 1531–1533, 1999.

Kaufman, A. J., and A. H. Knoll, Neoproterozoic variations in the C-isotopic composition of seawater: Stratigraphic and biogeochemical implications, *Precambrian Res.*, *73*, 27–49, 1995.

Kaufman, A. J., J. M. Hayes, A. H. Knoll, and G. J. B. Germs, Isotopic compositions of carbonates and organic carbon from upper Proterozoic successions in Namibia: Stratigraphic variation and the effects of diagenesis and metamorphism, *Precambrian Res.*, *49*, 301–327, 1991.

Kaufman, A. J., S. B. Jacobsen, and A. H. Knoll, The Vendian record of Sr and C isotopic Variation in seawater: implications for tectonics and paleoclimate, *Earth Planet. Sci. Lett.*, *120*, 409–430, 1993.

Kaufman, A. J., A. H. Knoll, and G. M. Narbonne, Isotopes, ice ages, and terminal Proterozoic earth history, *Proc. Natl. Acad. Sci. U.S.A.*, *94*, 6600–6605, 1997.

Kendall, C. G. St. C., and J. Warren, A review of the origin and setting of tepees and their associated fabrics, *Sedimentology*, *34*, 1007–1027, 1987.

Kennedy, M. J., B. Runnegar, A. R. Prave, K.-H. Hoffman, and M. Arthur, Two or four Neoproterozoic glaciations?, *Geology*, *26*, 1059–1063, 1998.

Kennedy, M. J., N. Christie-Blick, and A. R. Prave, Carbon isotopic composition of Neoproterozoic glacial carbonates as a test of paleoceanographic models for snowball Earth phenomena, *Geology*, *29*, 1135–1138, 2001a.

Kennedy, M. J., N. Christie-Blick, and L. E. Sohl, Are Proterozoic cap carbonates and isotopic excursions a record of gas hydrate destabilization following Earth's coldest intervals?, *Geology*, *29*, 443–446, 2001b.

Kent, D. V., and M. A. Smethurst, Shallow bias of paleomagnetic inclinations in the Paleozoic and Precambrian, *Earth Planet. Sci. Lett.*, *160*, 391–402, 1998.

Kirschvink, J. L., Late Proterozoic low latitude glaciation: The snowball earth, in *The Proterozoic Biosphere: A Multidisciplinary Study*, edited by J. W. Schopf and C. Klein, pp. 51–52, Cambridge Univ. Press, New York, 1992a.

Kirschvink, J. L., A paleogeographic model for Vendian and Cambrian time, in *The Proterozoic Biosphere: A Multidisciplinary Study*, edited by J. W. Schopf and C. Klein, pp. 569–581, Cambridge Univ. Press, New York, 1992b.

Kirschvink, J. L., E. J. Gaidos, L. E. Bertani, N. J. Beukes, J. Gutzmer, L. N. Maepa, and R. E. Steinberger, Paleoproterozoic snowball Earth: Extreme climatic and geochemical

global change and its biological consequences, *Proc. Nat. Acad. Sci. U.S.A.*, *97*, 1400–1405, 2000.

Knoll, A. H., Learning to tell Neoproterozoic time, *Precambrian Res.*, *100*, 3–20, 2000.

Koch, P. L., J. C. Zachos, and P. D. Gingerich, Correlation between isotope records in marine and continental carbon reservoirs near the Palaeocene/Eocene boundary, *Nature*, *358*, 319–322, 1992.

Krull, E. S., and G. J. Retallack, δ^{13}C depth profiles from paleosols across the Permian-Triassic boundary: Evidence for methane release, *Geol. Soc. Am. Bull.*, *112*, 1459–1472, 2000.

Kump, L., Interpreting carbon-isotope excursions: Strangelove oceans, *Geology*, *19*, 299–302, 1991.

Kump, L. R., and M. A. Arthur, Interpreting carbon-isotope excursions: Carbonates and organic matter, *Chem. Geol.*, *161*, 181–198, 1999.

Kvenvolden, K., Gas hydrates: Geological perspective and global change, *Rev. Geophys.*, *31*, 173–187, 1993.

Magaritz, M., R. B. Bär, A. Baud, and W. T. Holser, The carbon-isotope shift at the Permian/Triassic boundary in the southern Alps is gradual, *Nature*, *331*, 337–339, 1988.

McKenzie, D., Some remarks on the development of sedimentary basins, *Earth Planet. Sci. Lett.*, *40*, 25–32, 1978.

McKirdy, D. M., J. M. Burgess, N. M. Lemon, X. Yu, A. M. Cooper, V. A. Gostin, R. J. F. Jenkins, and R. A. Both, A chemostratigraphic overview of the late Cryogenian interglacial sequence in the Adelaide Fold-Thrust Belt, South Australia, *Precambrian Res.*, *106*, 149–186, 2001.

Meert, J. G., R. van der Voo, and S. Ayub, Paleomagnetic investigation of the Neoproterozoic Gagwe lavas and Mbozi complex, Tanzania and the assembly of Gondwana, *Precambrian Res.*, *74*, 225–244, 1995.

Meert, J. G., and R. van der Voo, Palaeomagnetic and ^{40}Ar/^{39}Ar study of the Sinyai Dolerite, Kenya: Implications for Gondwana assembly, *J. Geol.*, *104*, 131–142, 1996.

Miller, R. M., The Owambo basin of northern Namibia, in *African Basins*, edited by R. C. Selley, pp. 237–268, Elsevier Sci., New York, 1997.

Narbonne, G. M., A. J. Kaufman, and A. H. Knoll, Integrated chemostratigraphy and biostratigraphy of the Windermere Supergroup, northwestern Canada: Implications for Neoproterozoic correlations and the early evolution of animals, *Geol. Soc. Am. Bull.*, *106*, 1281–1292, 1994.

Padden, M., H. Weissert, and M. de Rafelis, Evidence for Late Jurassic release of methane from gas hydrate, *Geology*, *29*, 223–226, 2001.

Pavlov, A. A., J. F. Kasting, and L. L. Brown, Greenhouse warming by CH_4 in the atmosphere of early Earth, *J. Geophys. Res.*, *105*, 11,981–11,990, 2000.

Pavlov, A. A., J. F. Kasting, M. Hurtgen, and M. A. Arthur, A methane-rich Proterozoic atmosphere: possible link to the Neoproterozoic snowball Earth glaciations (abstract), *Eos Trans. AGU*, *82*(46), Fall Meet. Suppl., F347, 2001.

Petsch, S. T., and R. A. Berner, Coupling the geochemical cycles of C, P, Fe and S: the effect on atmospheric O_2 and the isotopic records of carbon and sulfur, *Am. J. Sci.*, *298*, 246–262, 1998.

Porada, H. R., The Khoabendus Formation in the area north-west of Kamanjab and in the southeast Kaokoveld, South West Africa, Geological Survey South Africa, South West Africa Ser., 4, 22 pp., Pretoria, 1974.

Prave, A. R., Tale of three cratons: tectonostratigraphic anatomy of the Damara orogen in northwestern Namibia and the assembly of Gondwana, Geology, 24, 1115–1118, 1996.

Prave, A. R., The Neoproterozoic Dalradian Supergroup of Scotland: An alternative hypothesis, Geol. Mag., 136, 609–617, 1999.

Purdy, E. G., Karst-determined facies patterns in British Honduras: Holocene carbonate sedimentation model, Am. Assoc. Petrol. Geol. Bull., 58, 825–855, 1974.

Riebesell, U., D. A. Wolf-Gladrow, and V. Smetacek, Carbon dioxide limitation of marine phytoplankton growth rates, Nature, 361, 249–251, 1993.

Sarg, J. F., Carbonate sequence stratigraphy, in Sea Level Changes: An Integrated Approach, Spec. Publ. 42, edited by C. K. Wilgus et al., pp. 155–181, Soc. Econ. Paleont. Mineral., Tulsa, Okla., 1988.

Sayles, R. W., Bermuda during the Ice Ages, Proc. Am. Acad. Arts Sci., 66, 382–467, 1931.

Schmidt, P. W., and G. E. Williams, Paleomagnetism of the Paleoproterozoic hematitic breccia and paleosol at Ville-Marie, Québec: Further evidence for the low paleolatitude of Huronian glaciation, Earth Planet. Sci. Lett., 172, 273–285, 1999.

Schrag, D. P., R. A. Berner, P. F. Hoffman, and G. P. Halverson, On the initiation of a snowball Earth, Geochem. Geophys. Geosyst., 3, 10.1029/2001GC000219, 2002. (Available at http://www.g-cubed.org)

Soffer, G., Evolution of a Neoproterozoic Continental Margin Subject to Tropical Glaciation: Tectonics, Stratigraphy, Geochemistry, and Sedimentology of the Otavi Group, NW Namibia, B.Sc. Thesis, Harvard College, Cambridge, Mass., 1998.

South African Committee for Stratigraphy (SACS), Damara Sequence, in Stratigraphy of South Africa, Part 1, Handbook Geol. Surv. S. Afr., 8, 415–438, 1980.

Stanistreet, I. G., P. A. Kukla, and G. Henry, Sedimentary basinal response to a Late Precambrian Wilson Cycle: The Damara Orogen and Nama Foreland, Namibia, J. Africa Earth Sci., 13, 41–156, 1991.

Summons, R. E., and J. M. Hayes, Principles of molecular and isotopic biogeochemistry, in The Proterozoic Biosphere, a Multidisciplinary Study, edited by J. W. Schopf and C. Klein, pp. 83–93 pp., Cambridge Univ. Press, New York, 1992.

Van Cappellen, P., and E. D. Ingall, Benthic phosphorus regeneration, net primary production, and ocean anoxia: A model of the coupled marine biogeochemical cycles of carbon and phosphorus, Paleoceanography, 9, 677–692, 1994.

Walter, M. R., J. J. Veevers, C. R. Calver, P. Gorjan, and A. C. Hill, Dating the 840–544 Ma Neoproterozoic interval by isotopes of strontium, carbon, and sulfur in seawater, and some interpretive models, Precambrian Res., 100, 371–433, 2000.

Ward, P. D., J. W. Haggart, E. S. Carter, D. Wilbur, H. W. Tipper, and T. Evans, Sudden productivity collapse associated with the Triassic—Jurassic boundary mass extinction, Science, 292, 1148–1151, 2001.

Wickham, S. M., and M. T. Peters, Oxygen and carbon isotope profiles in metasediments from Lizzies Basin, East Humboldt Range, Nevada: Constraints on mid-crustal metamorphic and magmatic volatile fluxes, Contribs. Mineral. Petrol., 112, 46–65, 1992.

Wilkinson, B. H., and J. G. C. Walker, Phanerozoic cycling of sedimentary carbonate, Am. J. Sci., 289, 525–548, 1989.

Williams, G. E., and P. W. Schmidt, Paleomagnetism of the Paleoproterozoic Gowganda and Lorrain formations, Ontario: Low paleolatitude for Huronian glaciation, Earth Planet. Sci. Lett., 153, 157–169, 1997.

Xiao, S., X. Yuan, A. J. Kaufman, H. Bao, and H. Wang, Neoproterozoic diamicitites and stable carbon isotope chemostratigraphy of the Quruqtagh series, NW China, Geol. Soc. Am. Abstr. Programs, 33, A-144, 2001.

Zachos, J. C., M. A. Arthur, and W. E. Dean, Geochemical evidence for suppression of pelagic marine productivity at the Cretaceous/Tertiary boundary, Nature, 337, 61–64, 1989.